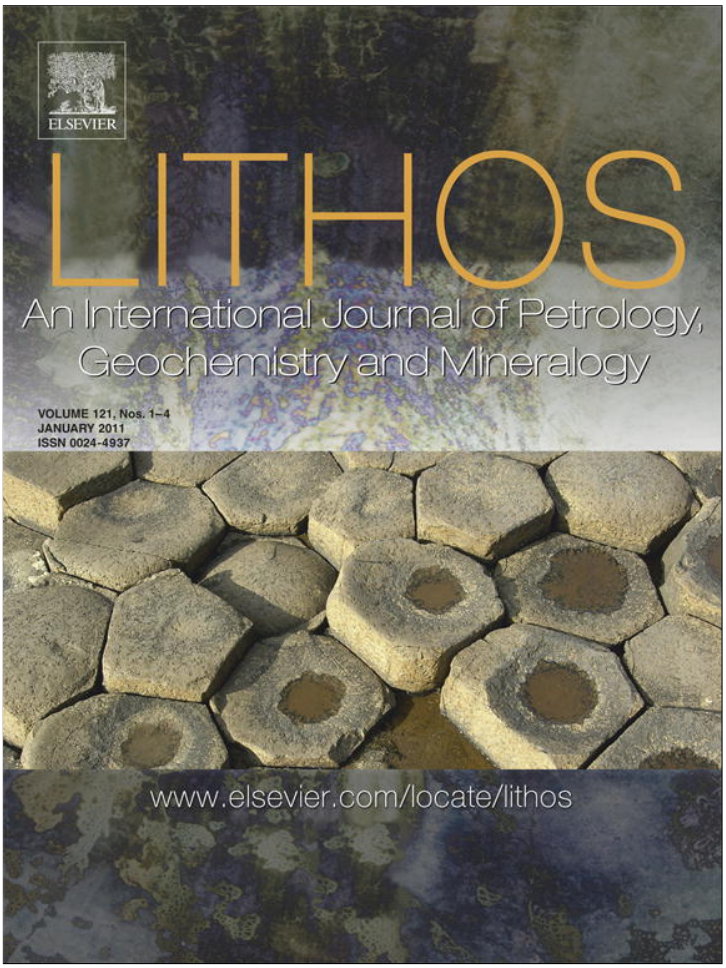

(This is a sample cover image for this issue. The actual cover is not yet available at this time.)

Lithos 134-135 (2012) 179–200

Contents lists available at SciVerse ScienceDirect

Lithos

journal homepage: www.elsevier.com/locate/lithos

Petrology of the Coyaguayma ignimbrite, northern Puna of Argentina: Origin and evolution of a peraluminous high-SiO_2 rhyolite magma

Pablo J. Caffe [a,b,*], Robert B. Trumbull [c], Wolfgang Siebel [d]

[a] CONICET, Argentina
[b] Instituto de Geología y Minería, Universidad Nacional de Jujuy, Av. Bolivia 1661, San Salvador de Jujuy, CP4600, Jujuy, Argentina
[c] GFZ German Research Center for Geosciences, Telegrafenberg 14473, Potsdam, Germany
[d] Institute of Geosciences, Universität Tübingen, Wilhelmstr, 56, 72074 Tübingen, Germany

ARTICLE INFO

Article history:
Received 5 September 2011
Accepted 27 December 2011
Available online 4 January 2012

Keywords:
Strongly peraluminous
SiO_2-rich rhyolite
Assimilation
Fractionation
Northern Puna
Central Andean plateau

ABSTRACT

The Coyaguayma ignimbrite is a strongly peraluminous (SP), sillimanite, garnet-bearing silicic rhyolite which erupted in the northern Puna segment of the central Andean plateau in the Upper Miocene (~11 Ma), a period that was characterized by the eruption of voluminous (100s to 1000s km^3) dacitic ignimbrites of high-K calc-alkaline affinity. In this region, the SP magmatic rocks are both rare and small, but their importance is potentially much greater as rocks of this type are usually interpreted as products of crustal melting and therefore useful for addressing mantle addition vs crustal recycling in the central Andes.

The phenocryst assemblage of the Coyaguayma ignimbrite comprises plagioclase (An26-18), quartz, Ba-rich and Ba-poor sanidine, minor Al-rich ferromagnesian minerals (Al^T- and Al^{VI}-rich biotite, almandine–spessartine garnet) and sillimanite, as well as accessory zircon and monazite. Textural relations suggest that the accessory and ferromagnesian phases crystallized before quartz and feldspars. Mineral equilibria suggest that crystallization of the rhyolite magma began at ~5 kbar and 800 °C, and continued almost isobarically to 720 °C, causing the residual liquid to increase H_2O contents from ~4–5% to ~7.5% before eruption.

Most major features (e.g., high SiO_2, A/CNK > 1.3, low CaO, MgO, TiO_2 and FeO) and trace element patterns (low Ba, Sr, Th, LREE and Eu/Eu*; high Rb, U, Y and Nb), along with the thermobarometric constraints on magmatic P, T and water contents are consistent with an origin by mica dehydration melting of metapelitic sources (e.g., typical biotite-muscovite gneisses from the outcropping S Puna basement). However, the relatively low initial $^{87}Sr/^{86}Sr$ (~0.7125), and high $^{143}Nd/^{144}Nd$ (~0.512200) ratios invalidate a pure crustal origin. Instead, we propose contamination of calc-alkaline dacitic magmas similar to typical Puna ignimbrites by metapelite at mid-crustal settings (≥18 km depth). Geochemical modeling that satisfies the chemical and isotopic data suggests mixing of 70% dacite and ~30% of metapelite partial melts, followed by extensive (70%) fractionation of plagioclase, K-feldspar, quartz and biotite, with minor magnetite and apatite from the hybrid magma. Sillimanite in the Coyaguayma rhyolite is interpreted as a restite mineral or a product of incongruent melting of the metapelite, which was preserved intact in the hybrid melt due to local equilibrium.

This petrogenetic model explains most characteristics of crystal-poor SP rhyolites from the Puna plateau (e.g., Tocomar, Ramadas rhyolites) and it may be more generally applicable to occurrences of SP magmas in Andean-type continental arcs dominated by calc-alkaline magmatism.

1. Introduction

The occurrence, petrogenesis and geotectonic significance of S-type, strongly peraluminous (SP) magmatic rocks, [in the sense of Miller (1985): Al_2SiO_5-, two mica-, garnet- or cordierite bearing "granitic" rocks] are still subjects of debate. While there is broad consensus that SP magmatic rocks require the participation of large quantities of crustal components in magma genesis, the actual processes involved are not always well understood. In the past, many SP rocks were considered the products of partial melting of entirely crustal (metasedimentary) protoliths (e.g., the S-type granites and volcanic rocks from the Lachlan Fold Belt in Australia). This view has been revised in the last 15 years to include the possibility of strong crustal contamination of mantle-derived magmas, based on experimental evidence (Castro et al., 2000; Díaz-Alvarado et al., 2011; Patiño Douce, 1999) and field, mineral and chemical data from SP granites in several regions (Collins, 1996; Elburg, 1996; Kontak and Clark, 1997; Sandeman and Clark, 2003, 2004). It is apparent that SP granitic magmas can form by more than one process but crustal melting is still regarded as a key ingredient. In some types of SP rocks it may be the sole or dominant process, in others

* Corresponding author. Tel./fax: +54 388 4221593.
E-mail addresses: pabcaffe@idgym.unju.edu.ar (P.J. Caffe), bobby@gfz-potsdam.de (R.B. Trumbull), wolfgang.siebel@uni-tuebingen.de (W. Siebel).

0024-4937/$ – see front matter © 2011 Elsevier B.V. All rights reserved.
doi:10.1016/j.lithos.2011.12.013

it may be one of several complementary processes (e.g., assimilation of crust by mantle-sourced hybrid magmas). In terms of geodynamic setting, SP magmatic rocks are most common in continental convergent settings, associated with thick crust and high-grade regional metamorphism (Chappell and White, 2001; Sylvester, 1998). The continental arc setting is less likely to produce SP magmas but where they do occur, the SP volcanic or plutonic rocks are potentially very useful for understanding the overall magmatic system as they give information on the chemical–mineralogic composition of the middle and lower crust.

The Miocene volcanic record in the central Andean plateau is characterized by extremely voluminous intermediate and silicic ignimbrite eruptions, especially in the region of the Altiplano–Puna Volcanic Complex (APVC) defined by de Silva (1989), which forms part of one of the largest ignimbrite provinces worldwide ($11–13\times10^3$ km^3; Kay et al., 2010a; Salisbury et al., 2011). Volcanic units with SP characteristics are scarce in this vast province (Fig. 1), and the same is true for mafic magmas, which are virtually absent in the APVC. However, just as the mafic magmas, the SP rocks from this region are particularly important for identifying end-member components involved in genesis of the much more common and voluminous intermediate dacites, which are well established as hybrid magmas of mixed mantle and crustal origin (e.g., Caffe et al., 2002; Guzmán et al., 2011; Kay et al., 2010a; Ort et al., 1996; Schmitt et al., 2001).

The APVC region is located in the Western Cordillera and southern Altiplano–northern Puna region, where intermediate and silicic magmatism is dominantly calc-alkaline and SP units are both rare and small in size. SP magmatic units are more common and larger in the Eastern Cordillera of Bolivia and Peru (Kari Kari ignimbrite, Schneider, 1987; Macusani volcanics, Pichavant et al., 1988a,b; Morococala Meseta ignimbrites, Morgan et al., 1998; Revancha dyke, Sandeman and Clark, 2003; Cayconi volcanic field, Sandeman and Clark, 2004; Los Frailes ignimbrites; Kay et al., 2010b). South of 20° S (Fig. 1) only a few outcrops of SP magmatic rocks are known and all of them are in the Argentine Puna. These are the Ramadas rhyolite (Gauthier et al., 1994; Viramonte et al., 1984, 2007), the Tocomar rhyolites (Petrinovic et al., 2006), and some units of the Pairique volcanic complex (Caffe et al., 2007), including the subject of this paper.

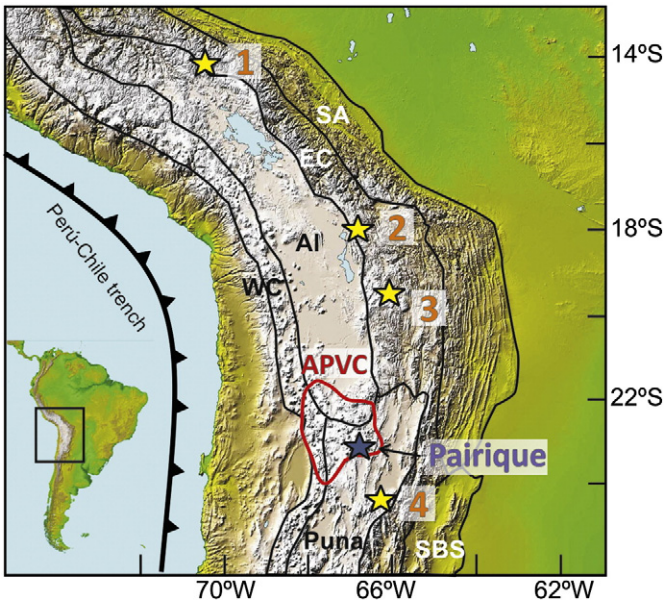

Fig. 1. Central Andes digital elevation model with location of the Pairique region and other occurrences (1–4) of SP Cenozoic volcanic rocks: 1 — Quenamari–Cayconi fields (Macusani ignimbrites; Revancha dyke; San Rafael pluton; Pachachaca, Jama-Jama and Cerro Cancahuine Formations); 2 — Morococala; 3 — Los Frailes–Kari Kari; 4 — Ramadas–Tocomar. Main morphotectonic divisions of the central Andes (WC: Western Cordillera; Puna; Al: Altiplano; EC: Eastern Cordillera; SBS: Santa Bárbara System; SA: Subandean Ranges), and the approximate location of the APVC (modified from de Silva, 1989), are also shown.
References from Caffe et al. (2007), Pichavant et al. (1988a), Sandeman and Clark (2003, 2004), Morgan et al. (1998), Kay et al. (2010b), Schneider (1987), Viramonte et al. (1984), and Petrinovic et al. (2006).

The Pairique area (Fig. 2) is a key region to study the petrogenesis of APVC magmas because here the intermediate calc-alkaline volcanic rocks are intercalated with a sequence of mafic lavas and related intrusive rocks, and with several SP magmatic units. Indeed, in this relatively small region of ~400 km^2 at least three different types of SP magmatic rocks were recognized (Caffe et al., 2007). This study focuses on one of these, a Miocene SP rhyolite unit named the Coyaguayma ignimbrite. This unit is geographically and temporally linked to, the Pairique volcanic complex, although not part of the Pairique eruptions per se. The Coyaguayma ignimbrite is distinct from the Pairique biotite–cordierite dacites by its high-SiO_2 and Al_2O_3-rich nature (expressed both in terms of mineralogy and rock composition), as well as by a less radiogenic Sr isotopic signature compared with the Pairique rocks. At the same time, the ignimbrite is compositionally similar to peraluminous rhyolites cropping out ~150 km to the south, in the southeastern edge of the northern Puna (Ramadas and Tocomar rhyolites, Fig. 1).

This paper presents new petrographic information with data from mineral and glass geochemistry and whole-rock major, trace element and isotopic analyses from the Coyaguayma ignimbrite, in order to deduce the petrogenesis and evolution of the rhyolitic magma. We discuss the most probable mechanisms involved in magma genesis, and compare the results with data from most of the best known SP volcanic rocks of the central Andes, especially those that crop out in nearby regions. The results have implications for understanding the petrogenesis and evolution of SP-type magmatism in the continental arc environment in general, and more specifically, the data contribute to understanding the "crustal end-member" involved in the genesis of the large-volume hybrid intermediate to silicic Altiplano–Puna magmas.

2. Methodology

Representative samples of the Coyaguayma ignimbrite were collected from different outcrops of the unit. Wherever possible, juvenile magmatic samples (pumice or cognate lithic clasts) were collected. Sampling of sufficient pumice fragments for bulk-rock analysis was not possible in all sites, so samples of the bulk ignimbrite were also analyzed. For the latter, a careful inspection was done after crushing the rock, in order to avoid accidental lithic fragments. Samples of pumice as well as bulk ignimbrite were used for textural and mineral chemistry studies. In whole rock geochemical studies the bulk ignimbrite compositions were used with due caution because of the potential bias from crystal sorting (see below).

Backscattered electron images of polished thin sections were taken in the Universidad Católica del Norte (Antofagasta, Chile), with a JEOL JSM 6360 scanning electron microscope under high vacuum conditions and applying an accelerating voltage of 25–30 kV.

Mineral and pumice matrix glass chemical analyses were carried out at the German Research Center for Geosciences (GFZ Potsdam) on a Cameca SX100 electron microprobe equipped with 4 wavelength-dispersive spectrometers. Automated data reduction and correction followed the PAP method (Pouchou and Pichoir, 1985). In all cases the accelerating voltage applied was 15 kV, whereas the electron beam size and intensity varied between 2 and 20 μm and 10 and 20 ηA depending on the phase to be analyzed. The element concentrations were obtained through calibration with natural and synthetic mineral standards of known compositions. Analytical uncertainties for the major components are considered to be better than 1–2% and for minor components better than 3–10%.

Whole rock chemical analyses (major elements, Rb, Ba, Sr, Nb, Zr, Y, Th, U, Sn, Pb, Cu, Cr and Ni) were determined by X-ray fluorescence

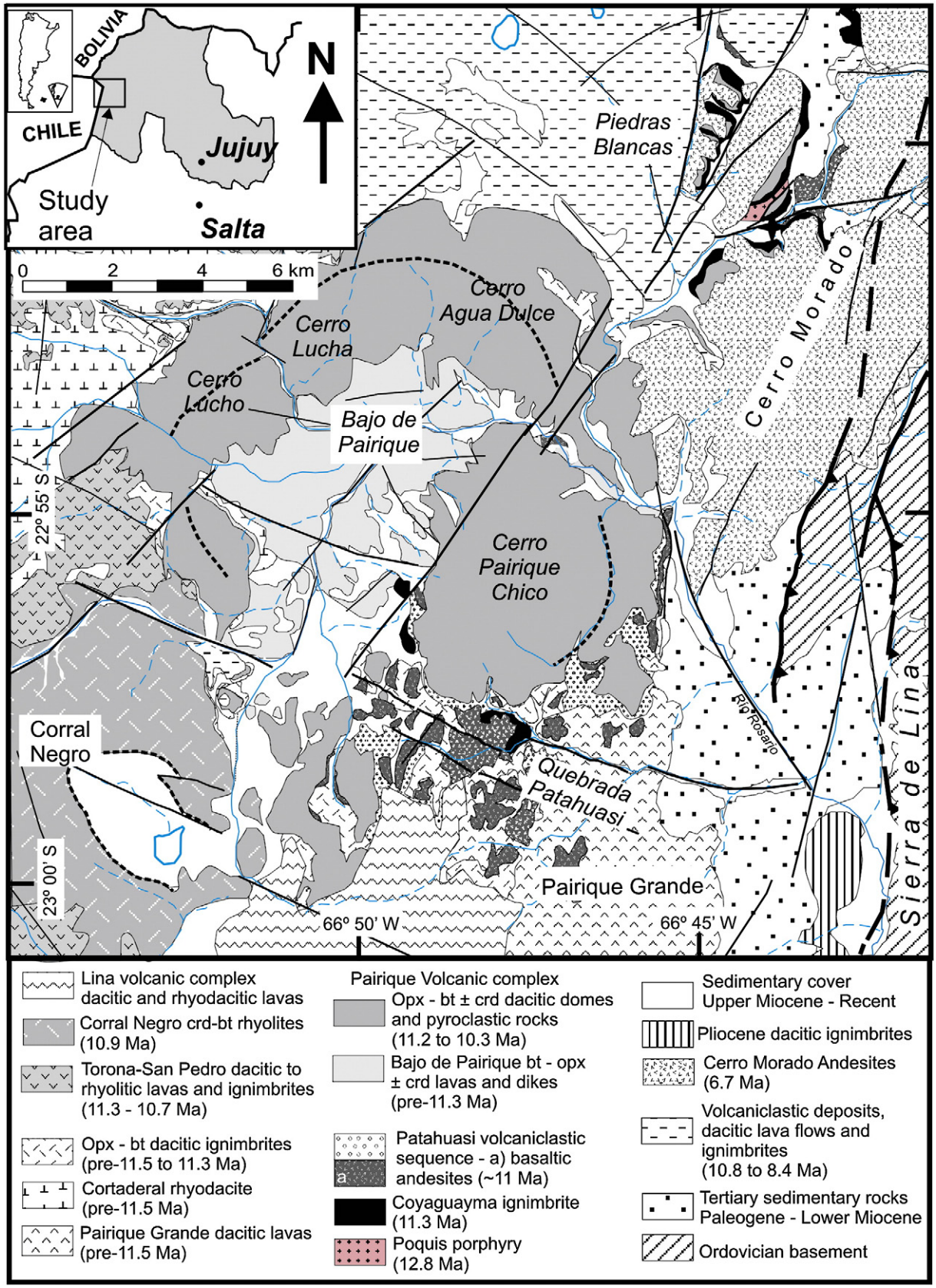

Fig. 2. Geological map of the Pairique region.
Modified from Caffe et al. (2007).

(XRF) in the Geochemistry Laboratory of the Instituto de Geología y Minería (Universidad Nacional de Jujuy), using a sequential Rigaku Rx2000 spectrometer. Details of XRF procedures are given in Caffe et al. (2002). Sample preparation in the Instituto de Geología y

Minería, Jujuy, employed agate mills to avoid contamination, and powers were homogenized in Retsch mixers. The rare-earth elements (REE) as well as Rb, Ba, Nb, Zr, Hf, Th, U, Co, Cr, Ni, Pb, and Sn were analyzed by ICP-MS in ALS-Chemex (Canada) Laboratories, using the same rock powders as for XRF analyses. The results for duplicate analysis by XRF and ICP-MS agreed within less than 10% relative.

Radiogenic isotope analyses on whole-rock samples were carried out at the University of Tübingen, Germany. For Sr and Nd, whole-rock powders were dissolved in 52% HF for four days at 140 °C on a hot plate. Digested samples were dried and redissolved in 6 N HCL, dried again and redissolved in 2.5 N HCl. Sr and the light rare earth elements were isolated from each other by standard ion exchange chromatography (Crock et al., 1984) with a 5-ml resin bed of AG 50W-X12 (200–400 mesh). Nd was separated from the other rare earth elements on quartz columns using 1.7-ml Teflon powder coated with HDEHP, di (2-ethylhexyl) orthophosphoric acid, as cation exchange medium (Richard et al., 1976). Isotopic data were obtained in static mode on a Finnigan MAT 262 mass spectrometer. The strontium fraction was dissolved in 1–2 μl of 2.5 mol HCl and loaded with a Ta-activator (Birck, 1986) onto a previously outgassed W-single filament and measured at 1300–1400 °C. Nd (as phosphate) was dissolved in 1 μl ultrapure H_2O and was measured as Nd^+ on a Re double filament configuration at temperatures between 1700 and 1800 °C. The $^{143}Nd/^{144}Nd$ ratios were normalized to $^{146}Nd/^{144}Nd = 0.7219$, and the $^{87}Sr/^{86}Sr$ isotope ratios to $^{86}Sr/^{88}Sr = 0.1194$. Analyses of three different loads of La Jolla standard gave $^{143}Nd/^{144}Nd$ ratios of 0.511859 ± 15, ($2\sigma_m$) while four analyses of the NBS 987 Sr standard yielded a $^{87}Sr/^{86}Sr$-ratio of 0.710238 ± 0.000019 ($2\sigma_m$) in good agreement with the certified values. Total procedural blanks (chemistry and loading) were 150 pg for Sr and 78 pg for Nd. εNd values were calculated using present day CHUR values of 0.1967 for $^{147}Sm/^{144}Nd$ (Jacobsen and Wasserburg, 1980) and 0.512638 for $^{143}Nd/^{144}Nd$ (Goldstein et al., 1984). Separation and purification of Pb was achieved on Teflon columns with a 100 μl (separation) and 40 μl bed (cleaning) of Bio-Rad AG1-X8 (100–200 mesh) anion exchange resin using a HBr–HCl ion exchange procedure (Manhès et al., 1978). Isotopic measurements were made by thermal ionization mass spectrometry on a Finnigan MAT 262 mass spectrometer. Pb was loaded with a Si-gel (Gerstenberger and Haase, 1997) onto a Re filament and measured at ~1300 °C in single-filament mode. A factor of 1‰ per mass unit for instrumental mass fractionation was applied to the Pb analyses, using NBS SRM 981 as reference material. The total procedural blank was 22 pg for Pb.

3. Regional geologic setting

The pre-Cenozoic basement in the northern Puna mainly comprises a weakly metamorphosed sequence of Ordovician shales, sandstones and submarine volcanic or intrusive igneous rocks of the same age. This sequence is part of the Cochinoca–Escaya Complex of Coira et al. (2004) and it builds up most of the major ranges of the area, including the north–south trending Sierra de Lina block which bounds the Pairique region to the east (Fig. 2). About 20 km to the north of Pairique, the Ordovician sequence is covered by rocks of the San Juan de Oro basin, which continues northwards in the southern Bolivian Altiplano basin. Ordovician rocks are thrust over Tertiary sedimentary rocks of Paleogene to Lower Miocene age (Fig. 2). Thrusting resulted from compressive stresses that probably acted from the Upper Oligocene to about 8 Ma, although volcanic rocks as old as 10–11 Ma in the area show evidence for only strike-slip deformation (Caffe et al., 2005, 2007). Strike-slip faulting developed through N–S, orogen-parallel and transverse structures (NE–SW, NW–SE and ~E–W), which apparently acted as preferential pathways for magma ascent during the Upper Miocene (Petrinovic et al., 2006).

The Pairique region lies on the eastern edge of the Altiplano–Puna Volcanic Complex (APVC) and contains an important record of basaltic andesite to rhyolite eruptions, mainly during the Upper Miocene (Fig. 2). Complete descriptions of units, ages and main eruptive vents in Pairique are given in Caffe et al. (2007). The volcanic activity peaked between ~11 and 9 Ma with the eruption of the Pairique volcanic complex, but it continued up to ~5 Ma, and well into the Pliocene in centers located ~15 km to the east. A characteristic of the Pairique area, which is otherwise uncommon in the northern Puna, is the recurrence of high-K calc-alkaline mafic volcanism alternating with intermediate to siliceous rocks including SP dacites and rhyolites. The garnet and sillimanite-bearing Coyaguayma ignimbrite is in the basal levels of this volcanic sequence.

4. Field relations and distribution of the Coyaguayma ignimbrite

The Coyaguayma ignimbrite comprises a group of pumice-rich pyroclastic flow deposits that are distributed along a narrow zone oriented N–S, to the east of the Pairique volcanic complex (Fig. 2). Directly to the northeast of Pairique, the ignimbrite overlies a series of small porphyritic rocks which Coira et al. (2004) correlated with the Poquis Porphyry (12.8 ± 0.5 Ma; Marinovic, 1979), and it is covered by block and ash flow deposits of 10.43 ± 0.03 Ma age (Caffe et al., 2007) from the Pairique volcanic complex (Figs. 2 and 3). In Quebrada Patahuasi, to the south of Pairique, the Coyaguayma ignimbrite covers the Pairique Grande lavas, whereas it onlaps the Bajo de Pairique lavas to the southeast of the Pairique volcanic complex (Caffe et al., 2007). The Coyaguayma ignimbrite also underlies a sequence of silicic volcaniclastic rocks and intercalated andesite lava flows and intrusive rocks (Patahuasi andesites; Fig. 2).

The $^{40}Ar/^{39}Ar$ age of this ignimbrite (isochron on biotite) is 11.28 ± 0.03 Ma (Caffe et al., 2005), establishing it as one of the oldest Cenozoic volcanic rocks in the Pairique region. At the type locality (Piedras Blancas, S 22° 50.252′–66° 44.391′ W), 3 km to the WNW of Rosario de Coyaguayma (Fig. 3), the Coyaguayma ignimbrite is composed of two unwelded flow units with a combined thickness of 18 m. The basal flow (5 m) comprises a gray, massive deposit rich (20–25%) in large, rounded pumice fragments up to 15 cm long set in a crystal-rich (>40%, Table 1) ash matrix. Large (average 10 cm long) fragments of the underlying rhyolitic porphyry and lithoclasts from the Ordovician basement are abundant (15%). The upper flow unit is whitish gray and exhibits vertical variations. The base (~2 m) is rich in pumice (15%) and lithic fragments (10%) up to 8 cm and 2 cm in size, respectively. This is followed upward by a 5 m thick massive deposit with pumice and lithic fragments which are smaller (1 cm and <2 cm in diameter, respectively) and less abundant (<8% and <2%) than in the base. The top of the section is characterized by high contents (50–70%) of small pumice clasts (to 4 cm), and by the presence of up to 5% of large clasts (0.5–10 cm) of rhyolite porphyry and Ordovician metapelites.

Approximately 15 km to the south of the type locality, in the Quebrada Patahuasi area (Fig. 2), the Coyaguayma ignimbrite is much thinner than in the type locality (<10 to 2 m), it comprises only a single flow unit that has smaller sizes of juvenile components (pumice <1 cm) and lithic fragments (<1% by volume and <2 cm size).

Based on its geographic distribution, field characteristics and lithic fragment size variation, Caffe et al. (2007) concluded that the Coyaguayma ignimbrite was erupted from a volcanic vent, probably buried, located toward the north or northwest of the Pairique area.

5. Petrography of the Coyaguayma ignimbrite

The Coyaguayma pumice is porphyritic with plagioclase, sanidine and quartz as the most abundant phenocrysts, and biotite (with minor garnet) representing ~2–5% (modal proportions as vesicule free or dense rock equivalent DRE, Table 1). The most abundant accessory mineral is sillimanite, followed in importance by traces of zircon

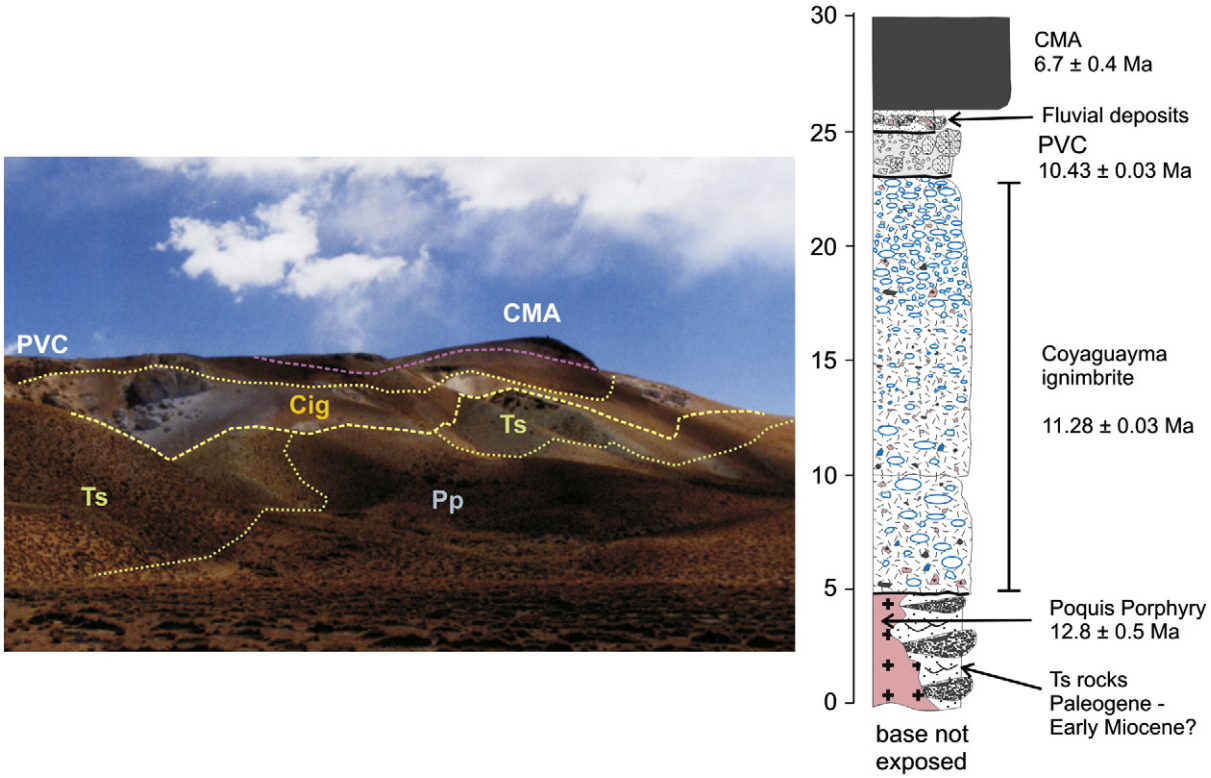

Fig. 3. Stratigraphic relations of the Coyaguayma ignimbrite (Cig) at Piedras Blancas (type locality). Ts: Tertiary sedimentary rocks. Pp: Poquis porphyry; PVC: Pairique volcanic complex block and ash deposits; and CMA: Cerro Morado Andesites.
Age data from Marinovic (1979), Coira et al. (1996), Caffe et al. (2005), and Caffe et al. (2007).

and monazite. Apatite is virtually absent, as are primary opaque minerals (Table 1). The pumice matrix appears fresh, the glass showing no signs of devitrification or microlites. The matrix of the ignimbrite resembles the pumice in terms of phenocryst abundance but it differs from the latter by having a higher proportion and more intense fragmentation of crystals (Table 1).

Plagioclase forms abundant (15–22% DRE, Table 1), fresh phenocrysts about 1–3 mm in size, and also rare microphenocrysts (0.3–0.5 mm) with scarce inclusions. The plagioclase shows a very slight optical zonation (Fig. 4a,b) which relates to variations in An contents (all mineral abbreviations are from Kretz, 1983). In some cases (e.g., sample PQ04-272p), clots of plagioclase having the same composition as the phenocrysts surround a few crystals cores with stronger zonation and probably higher An content (see below). Plagioclase commonly includes sillimanite, garnet, biotite and zircon.

Sanidine in the pumice and the ignimbrite matrix forms large (1–5 mm) euhedral to anhedral (Fig. 4c,d) phenocrysts which are fresh but commonly fractured. The phenocrysts are typically clear, with rare glass inclusions, and there is a weak optical zonation (Fig. 4d) and occasional embayed rims, mainly in the largely fragmented individual crystals (1.5–2.0 mm long). Inclusions of prismatic sillimanite may be arranged either randomly or along growth faces in the host crystal. Other inclusions comprise garnet, plagioclase, zircon, and rare, tiny biotite flakes. The DRE modal abundance of sanidine is slightly lower than that of plagioclase (Table 1).

Quartz is present in the same proportion as sanidine (Table 1). Crystals (0.3–4 mm) are euhedral to subhedral, and commonly contains glassy melt inclusions, which in turn host multiple bubbles and prismatic sillimanite (Fig. 5a). Some melt inclusions show negative crystal shapes, but most are elongated, adopting the shape of sillimanite grains that favoured their nucleation. Like sanidine, quartz also includes garnet and microlites of zircon. .

Biotite is the main ferromagnesian mineral in the pumice and ignimbrite matrix, but its abundance is always very low (Table 1). Biotite forms either large reddish-brown (0.7–1.8 mm) crystals or tabular microphenocrysts (0.1–0.5 mm), which are invariably fresh and flow-oriented. Some crystals are kinked (Fig. 6a) probably by strong shear during magmatic flow. Biotite contains inclusions of zircon, sillimanite and garnet, the compositions of which are similar to those of the respective isolated grains in the matrix. Sillimanite inclusions occur in the biotite rims and also in the cores, in which case, the sillimanite, like garnet, is surrounded by a thin film of glass (Fig. 6b).

Table 1
Representative pumice and bulk ignimbrite modal compositions.

Base 1200 points	Pumice		Bulk ignimbrite	
Sample	PQ01-40p	PQ04-272p	PQ01-40m	PQ02-133
# of analyses	3	2	3	3
Modal %				
Glass matrix	81.1	81.7	–	–
Qtz	3.5	4.7	10.5	11.5
Kfs	4.3	4.6	5.5	3.3
Pl	7.4	7.2	9.4	11.1
Bt	1.9	0.8	1.6	2.3
Gar	0.3	0.2	0.3	0.3
Sill	1.4	0.8	0.8	1.2
Ap	tr	tr	tr	0.1
Zrn–Mnz	0.1	tr	tr	tr
Op	–	–	0.1	0.2
Total crystals	18.9	18.3	28.2	30
Pumice	–	–	19.8	18.9
Glass shards	–	–	39.8	44.2
Lithoclasts	–	–	12.2	6.9
DRE crystals	37.8	36.6		

Modal compositions in pumice and bulk ignimbrite are shown without considering vesicles. Dense rock equivalent (DRE) crystals is the sum of crystals recalculated for 50 vol.% porosity in pumice.
Porosity is an average obtained from image analysis (Image Tool® software; Wilcox et al., 2002) on SEM photographs of pumice.

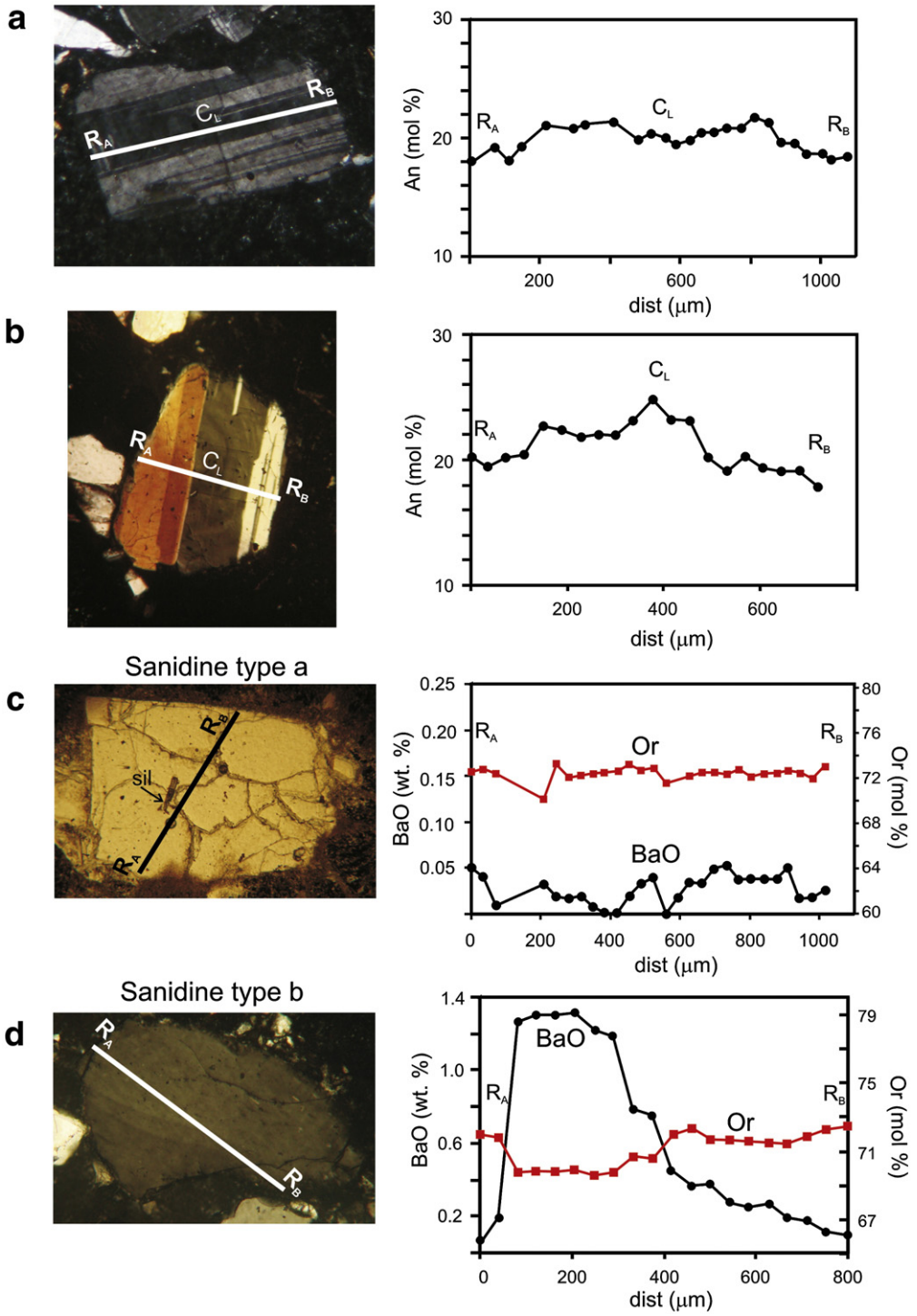

Fig. 4. Zoning profiles for feldspars. a–b) An in plagioclase; c–d) Or and BaO (wt.%) in low-Ba and high-Ba sanidines, respectively (see text for more details).

Garnet occurs as pale pink euhedral microphenocrysts (0.3–0.5 mm) of low modal abundance (Table 1). It formed relatively early in the crystallization sequence, preceeding all felsic minerals and perhaps some of the biotite. Near their rims, some garnet crystals include euhedral monazite and/or zircon (Fig. 6c). Where it forms discrete microphenocrysts in the pumice matrix, garnet appears perfectly stable, with no signs of reaction with the host melt.

As previously described, *sillimanite* occurs as tiny inclusions in all felsic phases and biotite (Figs. 5a and 6b), attesting to its early formation. Sillimanite also appears to be stable as microphenocrysts (0.2–0.5 mm long) and microlites in the pumice matrix glass (Fig. 5b). Sillimanite is uniform in appearance, represented by euhedral, locally thick (100–150 μm) elongated prismatic grains of variable size and degrees of fracturing (Fig. 6d). Fibrolitic sillimanite was not noted. Some grains in the ignimbrite matrix are fragmented and thus shorter than the more pristine crystals in pumice.

Apatite, *zircon* and *monazite* are present as microlitic accessory phases. Apatite is very rare, and was observed only in biotite from the ignimbrite matrix, never in pumice. The scarcity of apatite is in agreement with the very low P_2O_5 concentrations of matrix glass (see Section 7.1). Like apatite, monazite crystals are also rare, mostly occurring as inclusions in garnet (Fig. 6c) or, more rarely, as free

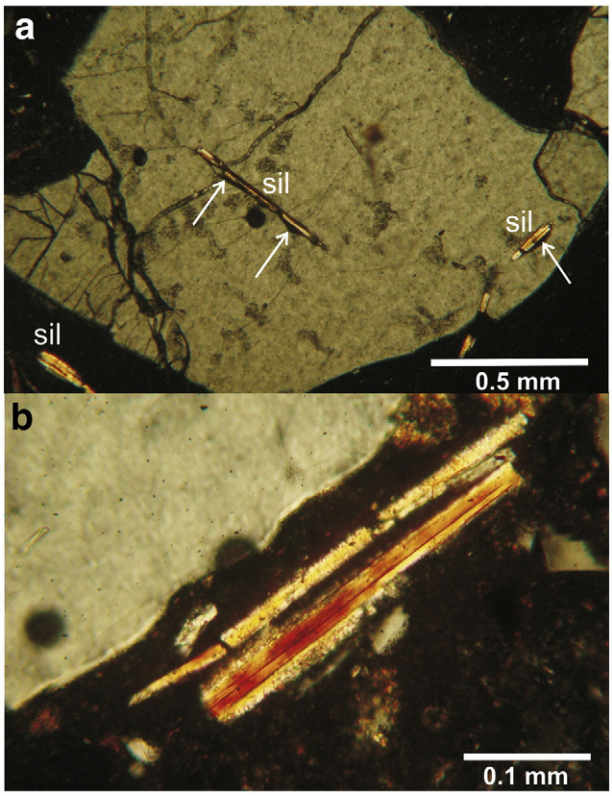

Fig. 5. a) Subhedral quartz phenocryst containing random inclusions of sillimanite (sil) surrounded by glass (arrows). Sample PQ01-40p. Crossed polars. b) Prismatic sillimanite crystals in the ignimbrite glassy matrix. Sample PQ01-35. Crossed polars.

microphenocrysts in the pumice glass (to 50–100 μm). Monazite includes, or is intergrown in epitaxis with much smaller (up to 20–30 μm, commonly <10 μm) grains of euhedral zircon (Fig. 6c), sometimes with very elongated shapes. The zircon apparently constitutes an early phase because it is included in all other minerals. Some zircon grains in the ignimbrite matrix are rounded and larger (>100 μm) than those in the pumice. They resemble zircons from the sedimentary and volcanic lithoclasts and are probably xenocrysts. This is supported by the rare observation of these rounded zircon grains alongside the more typical, euhedral and small zircons within the same biotite crystal.

6. Mineral compositions

6.1. Plagioclase

The predominant plagioclase composition is oligoclase (Table 2; Fig. 4a, b), with cores ranging from An_{18} to An_{26} (Or_{3-5}) and rims with the same compositional spread (An_{17-26}). Microphenocrysts in the ignimbrite matrix show almost the same range (An_{18}–An_{22}). Individual crystals show zoning (Fig. 4a) with normal to weakly oscillatory trends.

Quantitative analyses of the cores of monomineralic plagioclase clots are lacking, but qualitative SEM analysis showed that some cores are An-richer than the normal phenocrysts of the rock.

6.2. Sanidine

The mean composition of sanidine (Table 3) is $Or_{72\pm1.5}$, with the entire range from Or_{64} to Or_{74}. The BaO contents (Fig. 4c,d) discriminate two distinct groups, which correlate with two different textural types from pumice. The low BaO group (up to 0.12 mol% celsian component) comprises unfractured, generally euhedral pheno- and microphenocrysts lacking optical zonation and with oscillatory chemical zoning. The high BaO group (to 2.4 mol% celsian), comprises anhedral and fragmented crystals with striking optical zonation in what appears to be intermediate and rim zones. The low-Ba sanidines are consistent with the low Ba concentration in the bulk rock (60–70 ppm, Table 8). This group also shows no correlation between Ba concentration and the Or, Ab or An components. By contrast, in the high-Ba group, the high Ba contents correlate positively with the Al/Si ratio and negatively with Or, but there is no correlation with the An and Ab components.

6.3. Biotite

The trioctahedral micas in the Coyaguayma ignimbrite are Al-rich with average Mg# [100 $Mg/(Fe^{+2}+Mg)$] of 16 (Table 4). Almost all analyses plot in the siderophyllite corner (Fig. 7) of the classification diagram of Clarke (1981), similar to micas from highly evolved felsic rocks (e.g., granites from Central Spain and Macusani glasses). In the Abdel-Rahman (1994) diagrams, the biotites plot within the field of peraluminous granitoids (as appropriate for the host rock) or A-type granites depending on the diagram used (Fig. 7). In the Tischendorf et al. (1997) classification, the biotites classify as Fe-rich siderophyllite transitional to annite.

Coyaguayma biotite has elevated Al^{T} and Al^{VI}, contents, in keeping with the high Al_2O_3 saturation index of the rock. Compared to dark micas from other rhyolites in the region, the Coyaguayma biotites have strikingly high Al_2O_3 and low SiO_2 and TiO_2 concentrations (Table 4; Fig. 7). They are similar in this respect to biotites from Macusani glasses (Pichavant et al., 1988a) and from highly peraluminous granites with similar whole-rock SiO_2 concentrations (e.g., Hoyo de Manzanares and Cabeza Mediana plutons; Paredes da Beira and Jales granites; Neiva et al., 2002; Villaseca and Barbero, 1994, respectively). As commonly observed for Al-rich and Mg-poor biotites, the average Na content is high (~0.13 a.p.f.u.). The MnO and F concentrations are comparatively low (Table 4). Because of a lack of other F-bearing phases and the relatively low Mn content in garnet, we suggest that the low contents of these elements in biotite mainly reflects their low concentration in the magma and not competition with other fractionating phases (Table 8).

6.4. Garnet

Garnet is mainly a solid solution of almandine and spessartine (Alm_{81-87}; Sps_{10-12}), with very limited concentration of the pyrope and grossular components ($Prp_{4.4-5.3}$; $Grs_{0.4-2.2}$), and negligible Cr and Fe^{+3}_{calc} contents (Table 5). In the Miller and Stoddard (1981) diagram, the Coyaguayma garnet plots in the field of magmatic garnets at the low end of the spessartine range for the group (Fig. 8). The latter is consistent with the low Mn content of the bulk pumice and matrix glass of the rock. The garnet compositions are uniform, with slight oscillatory zoning of the grossular, almandine and pyrope components (Fig. 8). The Mg/Fe ratio of these garnets (Mg# 5–6) is lower than coexisting biotite which is a common characteristic of garnets from silicic peraluminous rocks (Villaseca and Barbero, 1994). The Coyaguayma garnet shows virtually no variation in MnO (Fig. 8). The lack of zoning suggests high crystallization temperatures (≥700 °C) for this mineral (see Dahlquist et al., 2007; and references therein).

In comparison with garnet from the Ramadas SP rhyolite (Fig. 8), the Coyaguayma garnet has a similar Mg# and lack of Mn zoning, but lower MnO contents (Ramadas: Sp_{23-24}; Gauthier et al., 1994). The latter is also true compared with magmatic garnets in peraluminous Pampean granites (e.g., Sp_{28-40}, Dahlquist et al., 2007). On the other hand, Coyaguayma garnets have higher spessartine and lower pyrope contents than garnet from peraluminous rhyodacites from the Lachlan Fold Belt (Clemens and Wall, 1984; Wyborn et al., 1981). Compared with garnet from calc-alkaline volcanic rocks

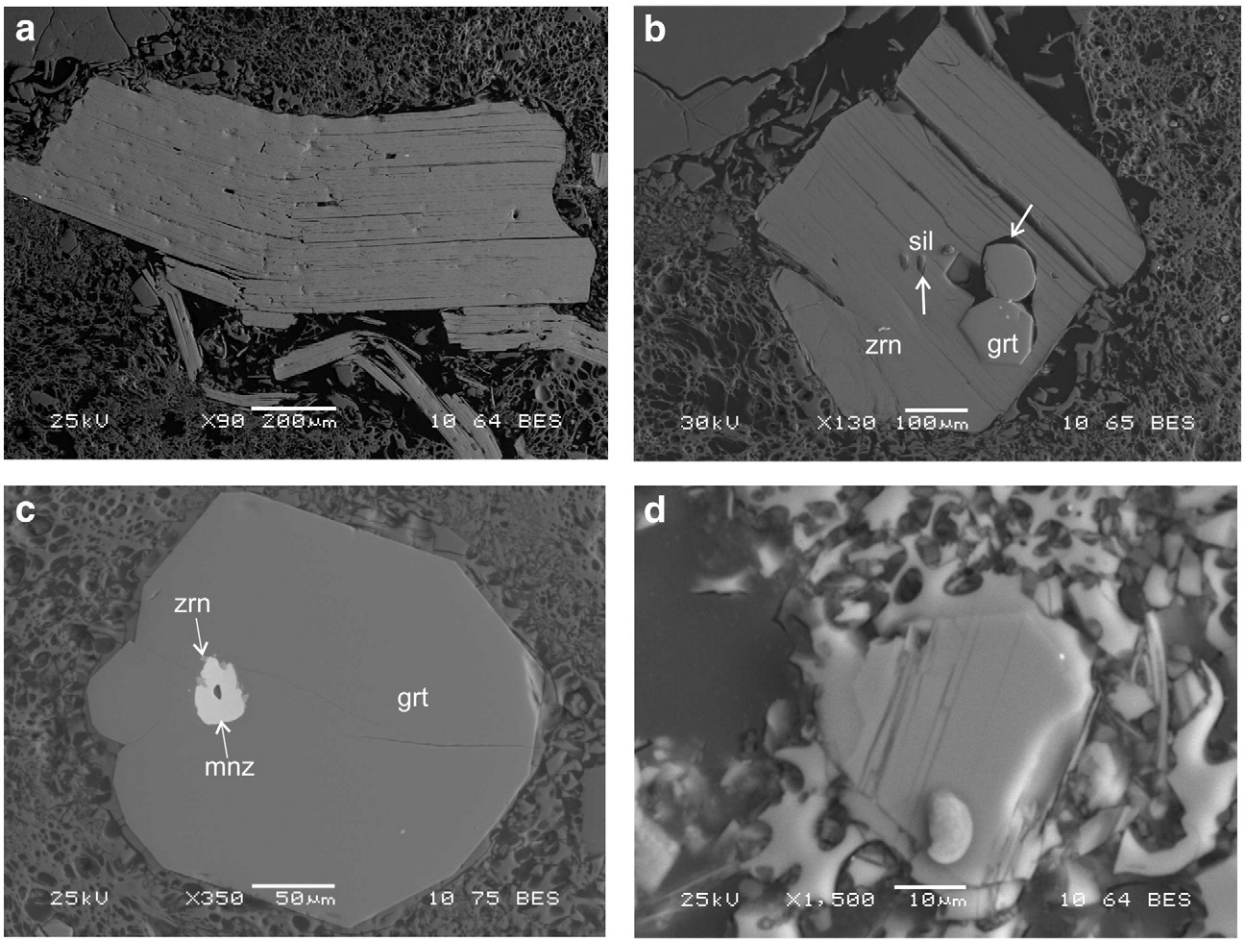

Fig. 6. Backscatter electron images of ferromagnesian and accessory phases from the Coyaguayma ignimbrite pumice (sample PQ01-40p). a) Bent and partially fragmented large biotite phenocryst. b) Inclusions of zircon (zrn), sillimanite (sil) and garnet (grt) in biotite; garnet and sillimanite are surrounded by a thin film of glass (arrows). c) Euhedral almandine garnet includes monazite (bright large mineral) with zircon (small gray microlites) in epitaxis. d) Basal section of a sillimanite crystal showing no reaction with the clean and fresh glassy groundmass.

(Harangi et al., 2001), the Coyaguayma compositions are substantially lower in grossular and pyrope components.

6.5. Sillimanite

Sillimanite approaches ideal Al_2SiO_5 composition, with only minor amounts of Fe (Table 6). The same is true for andalusite from metamorphic xenoliths in lavas of the Pairique volcanic complex (Caffe, unpublished data) and for magmatic Al_2SiO_5 from other central Andean peraluminous rocks (Morgan et al., 1998; Pichavant et al., 1988a). However, the Coyaguayma sillimanite has somewhat more Fe than fibrolite in the latter rocks.

Table 2
Representative microprobe analyses of plagioclase.

Sample	PQ01-40p						PQ02-133		
Crystal	Pl 9-1			Pl 10-1			Pl 9-1		
Point	9-pl 1c	9-pl 1i	9-pl 1r	10-pl 1c	10-pl 1i	10-pl 1r	9-pl 1c	9-pl 1i	9-pl 1r
SiO_2	61.59	61.83	62.49	62.23	61.98	63.98	64.31	63.12	62.44
Al_2O_3	24.27	23.50	23.22	23.29	23.32	22.08	23.09	23.48	22.58
FeO	0.02	0.06	0.05	0.03	0.02	0.18	0.06	0.03	0.07
BaO	bdl	bdl	0.01	bdl	bdl	bdl	0.02	0.01	bdl
CaO	5.45	4.88	3.95	4.26	4.72	3.77	4.05	4.40	4.02
Na_2O	8.66	8.89	9.48	9.15	8.98	8.69	9.44	9.11	9.16
K_2O	0.74	0.79	0.95	0.85	0.83	1.38	0.89	0.89	0.97
Total	100.73	99.95	100.15	99.81	99.85	100.08	101.86	101.04	99.24
Ab	71.2	73.4	77.1	75.8	74.0	74.4	77.0	75.2	76.2
An	24.8	22.3	17.8	19.5	21.5	17.8	18.2	20.0	18.5
Or	4.0	4.3	5.1	4.7	4.5	7.8	4.8	4.8	5.3

c — core; i — intermediate; and r — rim.
Calculation of Ab, An and Or after ion normalization to 32 O.

7. Whole rock geochemistry

7.1. Major elements

The Coyaguayma ignimbrite is a SiO_2-rich rhyolite (Table 8), in terms of pumice or bulk ignimbrite composition. The sum of alkalies is high ($Na_2O + K_2O$ 7–7.9%), as are the K_2O/Na_2O ratios (matrix ~1.5; pumice >2). Like other SiO_2-rich SP rhyolites from the central Andes (Macusani, Morococala, Ramadas, Tocomar; Morgan et al., 1998; Pichavant et al., 1988b; Petrinovic et al., 2006; Viramonte et al., 2007) the sum of FeO_t, TiO_2 and MgO (<2% in pumice; <2.2% in the bulk ignimbrite) and the CaO concentrations are very low (pumice <1%; ignimbrite <1.3%).

The SP geochemical character of the ignimbrite is shown by high values of the A/CNK_{mol} and A^* (Patiño Douce, 1992) indices, which are consistently higher in pumice than in the bulk ignimbrite (e.g., A/CNK_{pumice} 1.34–1.35; $A/CNK_{ignimbrite}$ 1.14–1.21; A^*_{pumice} >8, see Table 8). The high CIPW-normative corundum abundance (>4%) in pumice (Fig. 9) is similar to those observed in SP rocks elsewhere, somewhat higher than dacites and cordierite-bearing rhyolites from the region (e.g., Caffe et al., 2007; Morgan et al., 1998; Sandeman and Clark, 2003) and much higher than the calc-alkaline rhyolitic

Table 3
Representative microprobe analyses of sanidine.

Sample	PQ01-40p						PQ02-133		
Crystal	Type a			Type b			Type a		Mphc
Point	7-san 1c	7-san 1i	7-san 1r	14-san 3c	14-san 3i	14-san 3r	18-san 4c	18-san 4r	18-feld mc
SiO_2	65.47	65.44	66.02	64.97	63.96	66.64	65.36	65.35	63.95
Al_2O_3	19.01	18.95	18.92	19.19	19.17	19.22	18.85	18.99	18.19
FeO	0.01	0.04	0.06	0.05	0.06	0.03	0.03	0.04	0.11
BaO	0.02	0.04	0.05	0.04	1.31	0.18	0.01	bdl	0.02
CaO	0.12	0.10	0.10	0.11	0.15	0.13	0.12	0.15	0.24
Na_2O	2.94	3.00	3.01	3.16	2.99	3.12	3.14	3.20	2.98
K_2O	12.51	12.44	12.37	12.63	11.78	12.29	12.22	12.03	11.92
Total	100.08	100.01	100.53	100.15	99.42	101.61	99.73	99.76	97.41
Ab	26.2	26.7	26.9	27.4	27.0	27.6	27.9	28.6	27.2
An	0.6	0.5	0.5	0.5	0.7	0.6	0.6	0.7	1.2
Or	73.2	72.8	72.6	72.0	69.9	71.4	71.5	70.7	71.6
Cs	–	–	–	0.1	2.4	0.4	–	–	–

c — core; i — intermediate; r — rim; and Mphc — microphenocryst.
Calculation of Ab, An, Or and Cs after ion normalization to 32 O.

ignimbrites cropping out in neighboring areas of the APVC (e.g., Vilama, Purico and Toconao).

The pumice matrix glass has lower CaO, MgO, TiO_2 and FeO_t, and higher K_2O contents than the bulk pumice (Tables 7 and 8). The P_2O_5 and Na_2O contents in the bulk pumice plot between glass data from different samples (Fig. 9). The same is true for Al_2O_3 and normative corundum. For instance, in sample PQ02-133 normative corundum in the matrix glass is always lower than in bulk pumice (Fig. 9), but glass from sample PQ01-40p has higher normative corundum than bulk pumice. There are slight geochemical differences (including isotopic composition, see Table 8) between bulk pumice analyses from different sample sites, so it is likely that the ignimbrite represents the mixing of batches of magma that are mildly different in composition. Alternatively, there could have been more than one eruptive pulse from a compositionally evolving magma chamber.

7.2. Trace elements

The Coyaguayma pumice has high and uniform contents of Rb (333–369 ppm), U (13 ppm), Nb (26–31 ppm), Y (28–30 ppm), Pb (25–35 ppm) and Sn (10–13 ppm), and very low Sr (40–70 ppm), Ba (64–65 ppm), Th (8–9 ppm), Zr (51–54 ppm), total REE (77–82 ppm) and LREE (e.g., La = 12 ppm) concentrations (Table 8). In terms of several geochemical aspects, the bulk ignimbrite differs slightly from the pumice, which is consistent with the elutriation of glass shards during eruption and flow.

The trace element characteristics of the Coyaguayma ignimbrite resemble the most differentiated compositions from other peraluminous rhyolites in the central Andes, especially in terms of Sr, Th, U, Zr, Nb, total REE, Eu/Eu* and, to a lesser extent, Rb. The low concentrations of Ba seem to be a general characteristic of all the Puna SP rhyolites and some of the Ordovician anatectic leucogranites as well (e.g., Sola and Becchio, 2011). From all known Andean peraluminous volcanic rocks, the unit most similar to the Coyaguayma ignimbrite is the garnet-bearing Ramadas rhyolite.

The Coyaguayma ignimbrite exhibits a flat REE pattern (La/Yb <10) in chondrite normalized diagrams (Fig. 10), and a large negative Eu anomaly (Eu/Eu* ~0.3). The slopes of REE patterns are somewhat lower than those of the andalusite rhyolites from S Peru and Bolivia, but steeper and with a much smaller Eu anomaly than the highly fractionated macusanites, which were interpreted by Pichavant et al. (1987) as late-magmatic liquids from the Macusani ignimbrite

Table 4
Representative microprobe analyses of biotite.

Sample	PQ01-40p					PQ02-133				
Point	10-bt3	15-bt2	2-bt3	2-bt4	3-bt3	5-bt5	9-bt2	16-btinpl1	17-bt2	18-bt5
SiO_2	32.89	32.79	32.80	33.02	33.64	33.09	33.24	32.99	33.85	33.35
TiO_2	1.33	1.36	1.43	1.32	2.59	1.37	1.43	1.46	2.97	1.40
Al_2O_3	19.75	19.68	19.66	19.56	18.32	19.53	20.01	19.51	18.32	20.02
FeO	29.46	29.68	29.56	29.07	28.95	29.15	29.25	30.47	29.07	29.85
MnO	0.20	0.20	0.24	0.21	0.25	0.13	0.11	0.20	0.14	0.11
MgO	3.28	3.24	3.24	3.26	3.11	3.19	3.25	3.12	3.34	3.38
BaO	bdl	0.02	bdl	0.03	0.19	bdl	bdl	bdl	bdl	bdl
CaO	bdl	0.04	0.01	0.02	0.05	0.02	0.01	0.02	0.02	0.03
Na_2O	0.51	0.56	0.48	0.47	0.40	0.33	0.23	0.45	0.43	0.26
K_2O	8.77	8.64	8.72	8.63	8.27	8.80	8.95	8.64	8.78	8.86
F	0.51	0.58	0.49	0.50	0.52	0.59	0.68	0.59	0.66	0.62
Cl	0.48	0.55	0.48	0.55	0.58	0.55	0.45	0.44	0.53	0.48
Total	97.18	97.34	97.11	96.64	96.87	96.75	97.61	97.89	98.11	98.36
$O_{F—Cl}$	0.32	0.37	0.32	0.34	0.35	0.37	0.39	0.35	0.40	0.37
CTotal	96.86	96.97	96.79	96.30	96.54	96.38	97.22	97.54	97.71	97.99
Al^T	3.73	3.72	3.72	3.72	3.46	3.71	3.77	3.68	3.43	3.75
Al^{IV}	2.73	2.73	2.74	2.69	2.60	2.67	2.70	2.73	2.62	2.72
Al^{VI}	1.00	0.99	0.98	1.03	0.86	1.04	1.07	0.95	0.81	1.03
Li_2O_{calc}[a]	0.61	0.62	0.62	0.62	0.65	0.63	0.62	0.65	0.60	0.59
Na	0.16	0.16	0.15	0.15	0.13	0.10	0.07	0.14	0.13	0.08
Mg#	17	16	16	17	16	16	17	15	17	17

Ctotal: Corrected total.
Cations calculated after normalization to a 22 O basis. Mg# = Mg/Mg + Fe.
[a] Li_2O_{calc} is in %, calculated according to the equation $Li_2O = [2.7/(0.35 + MgO)] - 0.13$ from Tischendorf et al. (1997).

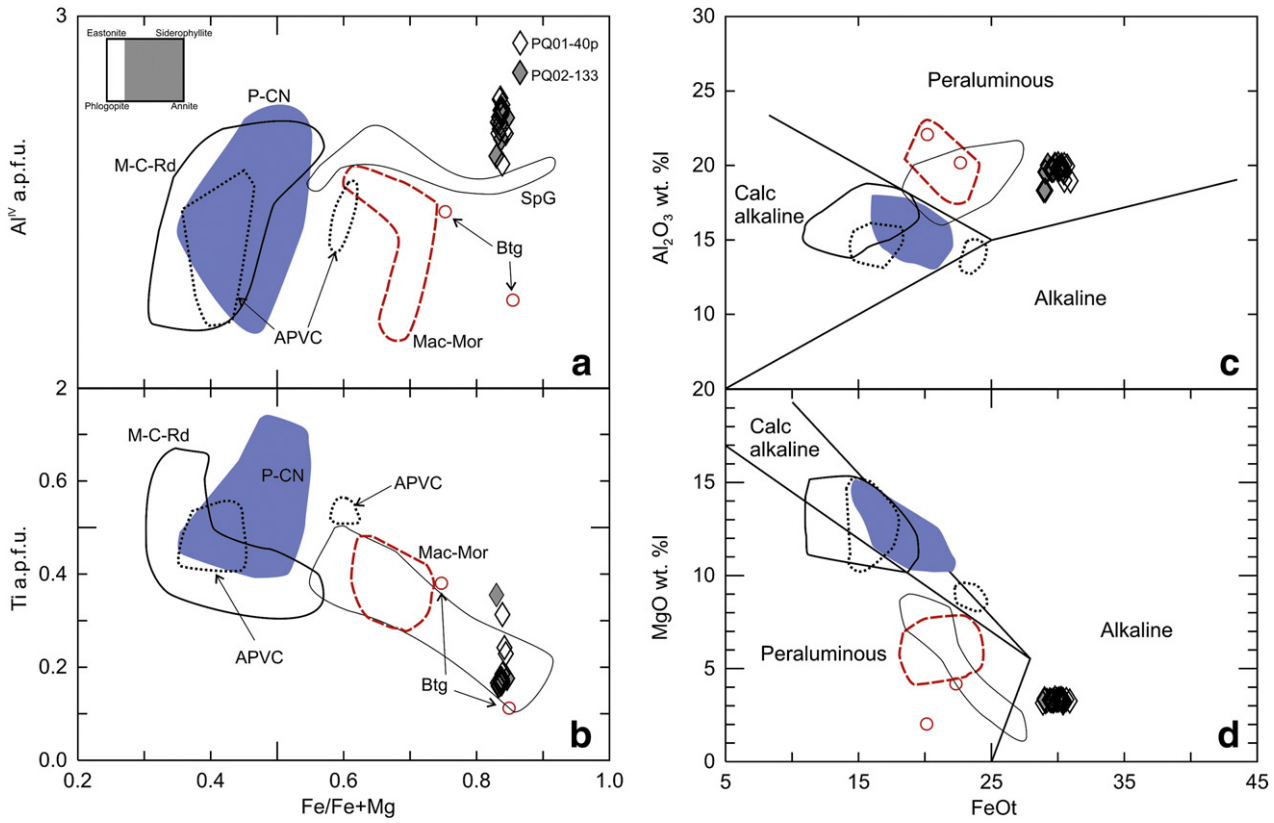

Fig. 7. a) Classification of Coyaguayma biotite in the Al^{IV} vs. Fe/Fe + Mg diagram of Clarke (1981). b) Ti (a.p.f.u.) vs. Fe/Fe + Mg plot for Coyaguayma ignimbrite biotite. c and d) Classification diagrams for biotites according to Abdel-Rahman (1994), with biotites from other SP and calc-alkaline magmatic units plotted for comparison: Mac–Mor, Macusani ignimbrites (Pichavant et al., 1988a) and Morococala rhyolites (Morgan et al., 1998); Btg, Macusanite glass (Pichavant et al., 1988a); SpG, peraluminous S-type granites from central Spain (Villaseca and Barbero, 1994); P–CN, Pairique volcanic complex and Corral Negro rhyolite (our own unpublished data); M–C–Rd, Minastira granite (Kontak and Clark, 1997), Cayconi volcanic rocks (Sandeman and Clark, 2004), and Revancha dyke (Sandeman and Clark, 2003); APVC, calkalcaline rhyolite ignimbrites from the APVC [Toconao and Tara, Lindsay et al. (2001); Vilama UCUb, Soler (2005); and Purico, Schmitt et al. (2001)].

magma. The REE abundances and distribution patterns of the Coyaguayma ignimbrite are practically identical to those of the nearby Ramadas and Tocomar rhyolites, apart from differences in the size or variability of negative Eu anomalies (Fig. 10).

7.3. Sr, Nd and Pb isotopes

Compared to other Miocene volcanic rocks (most of calc-alkaline affinity) from the northern Puna region (Fig. 11) the Coyaguayma

Table 5
Representative microprobe analyses of garnet.

Sample	PQ01-40p						PQ02-133			
Point	16-gt4c	16-gt4r	4-gt4c	4-gt4r	8-g1c	8-g1r	16-g2c	16-g2r	7-g2c	7-g2r
SiO_2	36.85	37.10	36.47	37.30	36.79	36.94	37.24	36.71	37.03	37.12
TiO_2	0.04	0.02	0.02	bdl	0.02	0.03	0.02	bdl	0.01	0.03
Al_2O_3	20.76	20.83	20.78	20.67	20.65	20.38	20.91	20.66	20.97	21.00
Cr_2O_3	bdl	bdl	bdl	bdl	bdl	bdl	bdl	0.02	0.04	bdl
FeO	36.96	36.54	36.05	35.97	36.28	36.49	36.18	36.39	35.84	35.64
MnO	4.25	4.46	4.58	4.51	4.84	4.51	4.59	4.57	4.98	4.73
MgO	1.13	1.12	1.20	1.12	1.12	1.10	1.10	1.12	1.10	1.12
CaO	0.80	0.77	0.72	0.71	0.69	0.69	0.70	0.74	0.73	0.70
Na_2O	0.03	0.07	0.04	0.05	0.04	0.06	0.03	0.03	0.03	0.03
Total	100.81	100.91	99.87	100.32	100.43	100.19	100.76	100.24	100.73	100.36
Fe_2O_{3calc}	0.30	–	0.27	–	0.19	–	–	0.12	–	–
Alm	83.3	83.0	82.3	82.8	82.3	82.8	82.8	82. 8	81.9	82.3
Adr	0.9	–	0.8	–	0.6	–	–	0.4	–	–
Grs	1.4	2.2	1.3	2.1	1.4	2.0	2.0	1.8	2.0	2.1
Prp	4.6	4.5	4.9	4.6	4.6	4.6	4.5	4.5	4.5	4.6
Sps	9.8	10.3	10.7	10.5	11.1	10.6	10.7	10.5	11.5	11.1
Uva	–	–	–	–	–	–	–	–	0.1	–
Mg#	5.2	5.3	5.6	5.3	5.2	5.1	5.2	5.2	5.3	5.3

c – core and r – rim.
Mg# = Mg / Mg + Fe. Fe_2O_{3calc} according to Droop (1987). Solid solution end members calculated following Rickwood (1968).
Symbols according to Kretz (1983).

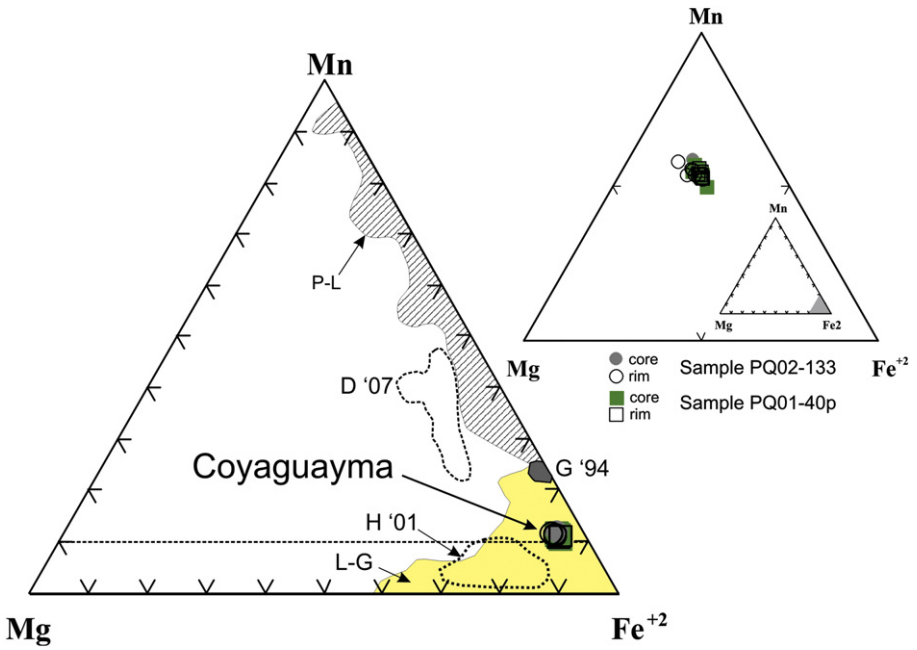

Fig. 8. Projection of garnet compositions from the Coyaguayma ignimbrite in the diagram of Miller and Stoddard (1981), with other magmatic garnets plotted for comparison: P–L, field for garnet in pegmatites and lavas (cavities). L–G, field for garnet phenocrysts in lavas and granites. H '01, garnet composition in calc-alkaline lavas (Harangi et al., 2001). G '94, garnet from the nearby Ramadas rhyolite (Gauthier et al., 1994). D '07, Mn-rich garnet from Peñon Rosado granite (Dahlquist et al., 2007). The smaller inset magnifies the Fe^{+2} corner of the main diagram to show the almost unzoned character of the Coyaguayma garnet.

pumice has slightly lower initial Sr ratios ($^{87}Sr/^{86}Sr_i$ 0.7125–0.7127). Overall, the Sr ratios are most similar to those of the Cerro Panizos ignimbrites (Ort et al., 1996) and the Lower Miocene volcanic dome complexes from the northern Puna (Caffe et al., 2002). However, the latter are calc-alkaline, they lack strongly peraluminous minerals, and their mineral, major and trace element compositions are very different from those of Coyaguayma pumice.

The relatively low $^{87}Sr/^{86}Sr_i$ values of the Coyaguayma pumice are even more apparent when compared with other SP Andean volcanic rocks (e.g., Pairique volcanic complex dacites; Corral Negro cordierite rhyolite; Ramadas and Tocomar rhyolites; Macusani ignimbrites; see Fig. 11). At the same SiO_2 content, the Coyaguayma Sr isotope ratios overlap the most radiogenic end of the range from the metaluminous Toconao ignimbrite (Lindsay et al., 2001). Compared with rocks from the Puna basement, the Coyaguayma Sr isotopic ratios overlap those of lower crustal xenoliths contained in the Salta Group basanites, plotting within the field defined for Paleozoic gneisses and granites from the Western Cordillera of Chile (Lucassen et al., 1999, 2001). A key point is that the Coyaguayma Sr isotope composition is less radiogenic than rocks from the local, Paleozoic Argentine basement.

In contrast to Sr, the Nd isotope ratios of the Coyaguayma ignimbrite (εNd −7.8 to −8.6) are much more similar to those of other peraluminous units from the Puna, such as the Tocomar (εNd −8.9 to −9.9) and Ramadas (εNd −8.0 to −8.1) rhyolites (Fig. 11), coinciding with the low radiogenic Nd signature shown by most volcanic rocks from the northern Puna and the outcropping basement. Cordierite-bearing rocks from the same area have slightly less radiogenic Nd isotope ratios, but are still comparable within error. Thus,

Table 6
Representative microprobe analyses of sillimanite and monazite.

Sample	PQ01-40p			PQ02-133
Point	6-sill 2	10-sill 4	8-mnz 1*	4-misc
SiO_2	37.15	35.89	4.61	37.02
TiO_2	bdl	bdl	0.04	0.03
Al_2O_3	62.46	61.69	2.89	63.11
FeO_t	0.42	0.48	1.60	0.48
MnO	bdl	0.01	bdl	bdl
MgO	0.01	bdl	0.05	bdl
BaO	0.02	bdl	0.02	0.04
CaO	0.01	0.01	1.25	0.02
Na_2O	0.02	0.05	0.07	0.04
K_2O	0.02	0.03	1.15	0.02
P_2O_5	0.01	0.05	26.79	0.14
Cl	0.03	0.02	0.03	0.02
F	nd	nd	1.00	nd
O_{F-Cl}	–	–	0.43	–
Total	100.14	98.22	39.07	100.91

8-mnz 1* monazite crystal included in garnet.

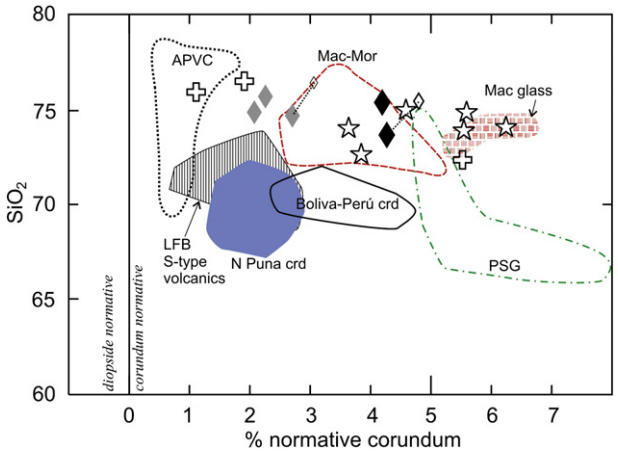

Fig. 9. Plot of normative corundum and SiO_2 for the Coyaguayma ignimbrite and other SP volcanic rocks from the Puna. Coyaguayma pumice (black diamonds) is more peraluminous than the matrix tuff (gray diamonds). Dotted tie lines link the compositions of glass (small open diamonds) and the whole rock. Tocomar (open stars) and Ramadas (crosses) ignimbrites generally show the same normative corundum contents, but some samples project into the field of macusanite (Mac glass). Plotted for comparison are the fields of calc-alkaline (APVC) high-SiO_2 rhyolites; cordierite rhyolites and dacites from Pairique (N Puna crd-bearing); Minastira granite, Revancha dyke and Morococala cordierite rhyolite (Bolivia–Peru crd); Macusani and Morococala andalusite rhyolites (Mac–Mor); Pampean S-type granites (PSG); and Lachlan Fold Belt S-type volcanic rocks (LFBv). References as in Fig. 7, except for PSG (Dahlquist et al., 2005) and LFBv (Clemens and Wall, 1984; Wyborn et al., 1981).

Table 7
Representative microprobe analyses of pumice matrix glass.

Sample	PQ01-40p						PQ02-133				
Point	1-gl	5-Pl gl	3-gl	5-gl	9-gl 6	9-gl 9	7-gl 1	11-gl 2	11-gl 2(2)	18-gl 1	18-gl 2
SiO_2	75.40	73.65	72.55	73.04	73.22	71.76	74.65	74.58	75.30	74.82	74.27
TiO_2	0.01	0.02	0.01	0.02	0.03	0.02	0.03	bdl	0.01	0.03	0.01
Al_2O_3	14.44	14.40	14.67	14.34	14.60	14.38	14.14	14.09	13.84	13.97	13.98
FeO_t	0.98	1.02	1.04	1.15	1.03	0.99	0.45	0.42	0.41	0.49	0.48
BaO	bdl	0.02	bdl	0.02	0.01	0.01	0.02	bdl	bdl	bdl	0.02
MnO	0.14	0.07	0.10	0.13	0.12	0.11	0.01	0.05	0.11	0.08	0.03
MgO	0.05	0.07	0.05	0.04	0.04	0.06	0.06	0.04	0.04	0.06	0.05
CaO	0.57	0.58	0.57	0.53	0.54	0.55	0.53	0.61	0.62	0.54	0.54
Na_2O	0.71	3.24	2.36	2.31	3.03	1.91	2.70	2.90	2.65	2.67	2.67
K_2O	3.35	4.47	4.70	4.76	4.46	5.00	5.21	5.05	5.10	5.27	5.18
P_2O_5	0.27	0.28	0.25	0.19	0.22	0.22	0.05	0.06	0.08	0.08	0.07
F	bdl	bdl	bdl	bdl	bdl	bdl	bdl	bdl	bdl	bdl	bdl
Cl	0.16	0.15	0.13	0.13	0.14	0.12	0.02	0.02	0.03	0.02	0.04
O_{F-Cl}	0.04	0.03	0.03	0.03	0.03	0.03	–	–	0.01	–	0.01
Total	96.00	97.94	96.40	96.67	97.41	95.10	97.87	97.82	98.18	98.03	97.33
A/CNK_{MOL}	1.29	1.45	1.47	1.45	1.35	1.50	1.28	1.24	1.26	1.26	1.27
A^*	8.56	8.61	8.79	8.61	8.75	8.72	8.45	8.32	8.09	8.32	8.38

A^* is the alumina saturation index corrected for alkalis, as proposed by Patiño Douce (1992).

the isotopic resemblance between the basement and Coyaguayma ignimbrite is stronger with respect to Nd than to Sr. However, the Coyaguayma rocks have much higher Sm/Nd ratios than the basement rocks (and about twice the values of most volcanic rocks from the region). This characteristic, expressed by flat normalized REE patterns, is shared by the other northern Puna SP rhyolites and by some Paleozoic leucogranites from the basement as well (e.g., Elortegui Palacios et al., 2011; Sola and Becchio, 2011).

The Pb isotope ratios of the Coyaguayma ignimbrite are coincident with the northern Puna Ordovician basement rocks (Fig. 12) and they overlap the field of N Chile basement as well (Lucassen et al., 2001, 2002). However, there is no coincidence of Pb ratios with the Salta Rift granulite xenoliths. Like other Puna magmatic units, the $^{207}Pb/^{204}Pb$ and $^{208}Pb/^{204}Pb$ ratios of Coyaguayma ignimbrite plot above the Stacey and Kramers (1975) Pb growth line. The Coyaguayma has very radiogenic $^{206}Pb/^{204}Pb$ ratios, higher than the Tocomar rhyolites and partially overlapping the cordierite-bearing volcanic rocks from the northern Puna. Like with Sr and Nd, the Coyaguayma Pb ratios overlap within error those of the northern Puna 20–16 Ma volcanic units and Panizos rocks, but in contrast to Sr and Nd, the Pb ratios are also coincident with metapelite xenoliths hosted in Pairique dacites (sample PQ02-90B, Table 8). The $^{206}Pb/^{204}Pb$ ratios are less radiogenic than those of the Atana and Toconao ignimbrites. For a given value of $^{206}Pb/^{204}Pb$, the Coyaguayma ignimbrite shows intermediate $^{208}Pb/^{204}Pb$ ratios, plotting between those of the Panizos ignimbrite (lower) and most of the other volcanic rocks which have higher $^{208}Pb/^{204}Pb$ ratios. The Tocomar rhyolites have strikingly low $^{208}Pb/^{204}Pb$ ratios. .

8. Mineral equilibria and physico-chemical conditions of crystallization

The mineralogy and whole rock composition of the Coyaguayma ignimbrite are amenable to the evaluation of the P–T conditions of magma crystallization through application of various geothermometers and barometers, and to make a preliminary estimate of the pre-eruptive volatile contents.

8.1. Zr saturation temperature (T_{Zr})

The estimation of magmatic temperatures from the zircon saturation method T_{Zr} (Watson and Harrison, 1983) yields 722° to 731 °C for pumice , and higher T_{Zr} (715–751 °C) for the bulk ignimbrite (Table 9). The latter value has little petrologic meaning, as some xenocrystric zircon in the matrix may result from the dissaggregation of lithoclasts, and Zr concentration may also have increased by the loss of vitric shards by elutriation during flow. The Coyaguayma pumice contains small (a few μm) free grains of euhedral zircon in the vicinity of phenocrysts of the main rock-forming minerals, and there seem to be few, if any, inherited zircon crystals similar to those present in the lithoclasts. The garnet–biotite geothermometer yields much higher temperatures than T_{Zr}, whereas two-feldspar equilibrium temperatures are similar or slightly higher than T_{Zr} (see Sections 8.2 and 8.4). Textural relationships indicate that zircon formed earlier than garnet, biotite, and feldspars. Therefore, either the bulk magma was not saturated in $ZrSiO_4$ and zircon crystallization was due to local saturation in the vicinity of precipitating major silicates (e.g., Bea, 1996); or the original Zr concentration in the magma was lowered by zircon sequestration during fractionation of major silicates. In both cases, the calculated T_{Zr} would underestimate the real liquidus temperature of the magma.

8.2. Garnet–biotite temperature (T_{GB})

There are many calibrations for the temperature relation of Fe–Mg cation exchange between garnet and biotite, and these yield quite variable results (Ferry and Spear, 1978; Ganguly and Saxena, 1984; Hodges and Spear, 1982; Holdaway, 2000; Kaneko and Miyano, 2004; Pigage and Greenwood, 1982; among others). If all these models are applied to the Coyaguayma mineral compositions, the temperature estimates vary over 200 °C. Calculations of T_{GB} <700 °C were discarded, because the lack of zoning in garnet (see above) imply that magma temperatures were at least 700 °C (Dahlquist et al., 2007, and references therein). Also, in a rhyolitic magma with moderate F (~0.5% in biotite and 300–600 ppm in whole rock) and relatively high H_2O contents (see Section 8.5), the stable coexistence of sillimanite and K-feldspar and the absence of muscovite at the estimated pressure of crystallization (6–4 kbar, see Section 8.3) indicates temperatures above 680–700 °C (cf. Clarke et al., 2005). This is consistent with the ≥700 °C equilibrium temperatures calculated for plagioclase-sanidine (see below), which are texturally later than garnet and biotite. Some garnet–biotite calibrations yield temperatures unrealistically high for the Coyaguayma ignimbrite. Thus, the Pigage and Greenwood (1982) and Ganguly and Saxena (1984) thermometers yielded ≥850°–890 °C (Table 10), which are similar to estimates for the considerably more mafic Pairique dacites (Caffe and Trumbull, 2006). As pointed out by Anderson (1996), the Ganguly and Saxena calibrations are best applied for garnet rich in MnO,

Table 8
Whole rock analyses of Coyaguayma ignimbrite and pumice, and metamorphic xenoliths of northern Puna volcanic rocks.

Sample	PQ01-40p[a]	PQ04-272p[a]	PQ02-133[b]	PQ02-97[b]	PQ02-97L[c]	PQ02-131[d]	PQ02-90B[d]	P-150[e]
SiO_2	74.18	72.26	73.22	74.05	75.44	53.21	53.36	47.33
TiO_2	0.05	0.04	0.10	0.09	0.05	0.86	1.11	1.14
Al_2O_3	14.54	15.33	14.04	14.00	13.85	23.79	23.51	29.7
Fe_2O_3	1.29	1.50	1.54	1.46	1.36	8.41	6.03	7.52
MnO	0.06	0.05	0.03	0.06	0.02	0.08	0.05	0.07
MgO	0.10	0.25	0.73	0.33	0.29	2.57	2.50	2.48
CaO	0.76	0.81	1.32	1.21	0.93	0.62	5.32	1.29
Na_2O	2.40	2.54	2.65	3.05	3.30	1.87	4.17	2.07
K_2O	5.01	5.33	4.47	4.68	4.44	6.18	2.89	6.24
P_2O_5	0.17	0.15	0.11	0.15	0.14	0.14	0.17	0.21
F %	0.03	0.06	0.05	n.a.	n.a.	0.02	n.a.	n.a.
LOI	2.32	2.40	2.45	1.59	0.82	2.88	1.21	1.07
Total	100.89	100.71	100.70	100.65	100.63	100.64	100.32	99.11
Mg#	13	25	48	31	30	38	45	38
A/CNK_{MOL}	1.35	1.34	1.21	1.14	1.16	2.18	1.20	2.24
A*	8.26	8.78	7.23	7.41	7.60	14.85	8.00	17.90
B (ppm)	82	83	41	n.a.	n.a.	90	n.a.	n.a.
Li	16	19	23	n.a.	n.a.	103	n.a.	n.a.
Ba	64	65	358	306	105	950	667	1860
Rb	369	333	238	206	271	186	114	148
Sr	70	41	168	135	58	74	475	713
Y	28	30	25	31	33	31	35	45
Zr	54	54	88	72	51	134	201	225
Hf	3	3	3	2	2	4	5	7
Nb	32	32	18	19	26	15	20	21
Th	8	9	11	10	9	14	21	27
U	13	13	7	7	12	5	5	6
Co	65	51	44	50	27	34	38	40
Cr	bdl	57	5	1	30	71	119	120
Ni	bdl	20	4	11	10	40	28	n.a.
Cu	bdl	6	1.9	10.4	35	177.3	n.a.	n.a.
Sn	12.8	10	1.9	6.8	14	1.7	n.a.	5
Pb	35.4	26	29.3	32.8	35	26.7	20.5	n.a.
La	12.5	12.2					69.2	73.4
Ce	29.4	28					141.5	151
Pr	3.6	3.4					16.1	17.3
Nd	13.2	12					58.8	64.2
Sm	4.6	4.2					11.6	13
Eu	0.5	0.4					3.8	2.7
Gd	5	4.5					9.8	11
Tb	1.1	1					1.4	1.7
Dy	6.4	5.8					7.7	10.1
Ho	1.1	1					1.5	2
Er	2.6	2.4					4.1	5.5
Tm	0.3	0.3					0.6	0.8
Yb	1.8	1.7					3.6	5.3
Lu	0.2	0.2					0.6	0.9
Eu/Eu*	0.32	0.28					1.10	0.70
$^{87}Sr/^{86}Sr$	0.715128 ± 10	0.716313 ± 9					0.720378 ± 9	0.718729 ± 7
$^{87}Rb/^{86}Sr$	15.26	23.52					0.70	0.60
$^{143}Nd/^{144}Nd$	0.512240 ± 7	0.512200 ± 7					0.512023 ± 8	0.512086 ± 11
$^{147}Sm/^{144}Nd$	0.2115	0.2125					0.1197	0.1229
$^{206}Pb/^{204}Pb$	18.877	18.928					18.885	n.a.
$^{207}Pb/^{204}Pb$	15.678	15.665					15.668	n.a.
$^{208}Pb/^{204}Pb$	38.992	39.020					39.047	n.a.

A* is the alumina saturation index corrected for alkalis (Patiño Douce, 1992).
Samples PQ02-133, PQ02-97, PQ02-97L and PQ02-131 not analyzed for REE and isotopes.
The isotopic composition of sample P-150 was obtained at the Institute of Earth Sciences-Academia Sinica (Taipei, China); methodology as in Kay et al. (2010a).
[a] Pumice.
[b] Bulk ignimbrite.
[c] Cognate lithic fragment.
[d] Metamorphic xenolith (Pairique).
[e] Metamorphic xenolith (Pan de Azúcar).

which is not the case here. For these reasons and because of the similarity of experimental garnet compositions with those in Coyaguayma ignimbrite (low X_{Mn} and X_{Ca}; see Anderson, 1996), we prefer the Ferry and Spear (1978) and Hodges and Spear (1982) calibrations. These calibrations result in a tight range of values, 780–790 °C, using the average compositions of garnet and biotite cores (Table 10). We consider these values as a good estimate of the mean temperature of equilibrium between these two minerals, and consequently the highest temperature recorded by the Coyaguayma ignimbrite magma.

8.4. Two-feldspar thermometry (T_{2fsp})

The Solvcalc software (Nekvasil and Wen, 1994) was used for calculating T_{2fsp}, applying the Green and Usdansky (1986), Fuhrman and Lindsley (1988) and Elkins and Grove (1990) solution models (T_{G-U};

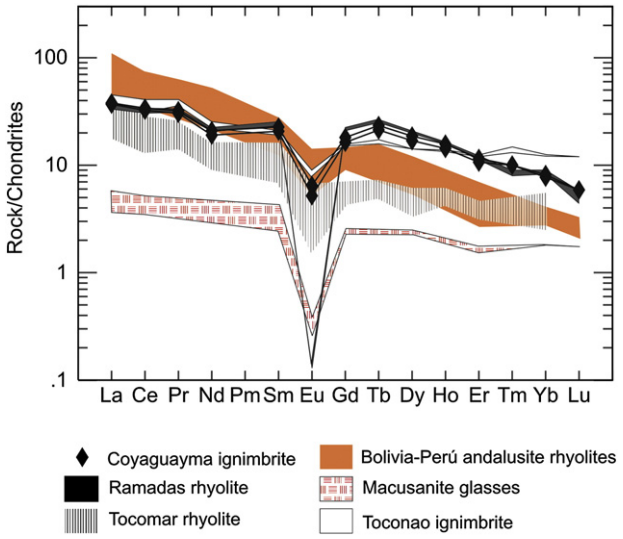

Fig. 10. Chondrite-normalized REE diagram showing the Coyaguayma ignimbrite pumice compared with other central Andes SP volcanic rocks. The metaluminous high-SiO_2 Toconao ignimbrite (Lindsay et al., 2001) was interpreted as a residual liquid fractionated from the Atana dacitic magma. References as in Fig. 7. Normalization values from Nakamura (1974).

T_{F-L}; T_{E-G}, respectively). The only K-feldspars used in calculations were the more common low-Ba sanidines, which seem to be the more reasonable compositions for magmatic sanidines in equilibrium with the low-Ba bulk composition (see Section 6.2). The solutions for feldspar pairs whose temperatures differ by ≥10 °C for Ab, An and Or, were excluded from the mean T_{2fsp} calculation (Table 11).

Since the two-feldspar equilibrium is pressure-dependent, T_{2fsp} temperatures were calculated at 5 and 3 kbar, which results in a wide range of values (772–649 °C, Table 11). There are systematic differences among the solution models ($T_{G-U} > T_{F-L} > T_{E-G}$), which are more pronounced at the 5 kbar pressure, but the total range is typically within the 50 °C uncertainty of the method (Kroll et al., 1993). Considering the mean values and standard deviations, the results of all two-

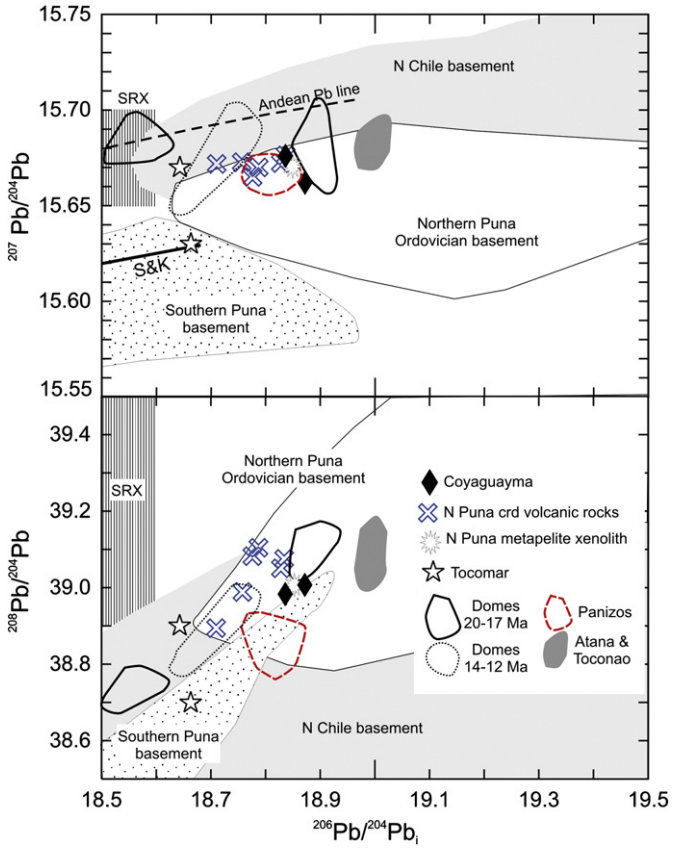

Fig. 12. $^{207}Pb/^{204}Pb_i$ and $^{208}Pb/^{204}Pb_i$ versus $^{206}Pb/^{204}Pb_i$ plots for the Coyaguayma ignimbrite pumice and northern Puna xenoliths. Shown for comparison are initial Pb isotopic ratios of the SP Tocomar rhyolites (Petrinovic et al., 2006), northern Puna volcanic domes (Caffe et al., 2002), northern Puna cordierite rhyolites and dacites (authors' unpublished data), Panizos (Ort et al., 1996) and Atana and Toconao ignimbrites (Lindsay et al., 2001). Andean Pb line and fields for N Chile basement, Salta Rift xenoliths (SRX), northern Puna Ordovician rocks, and southern Puna basement are based on Lucassen et al. (2001, 2002). S&K is Stacey and Kramers (1975) Pb reference line.

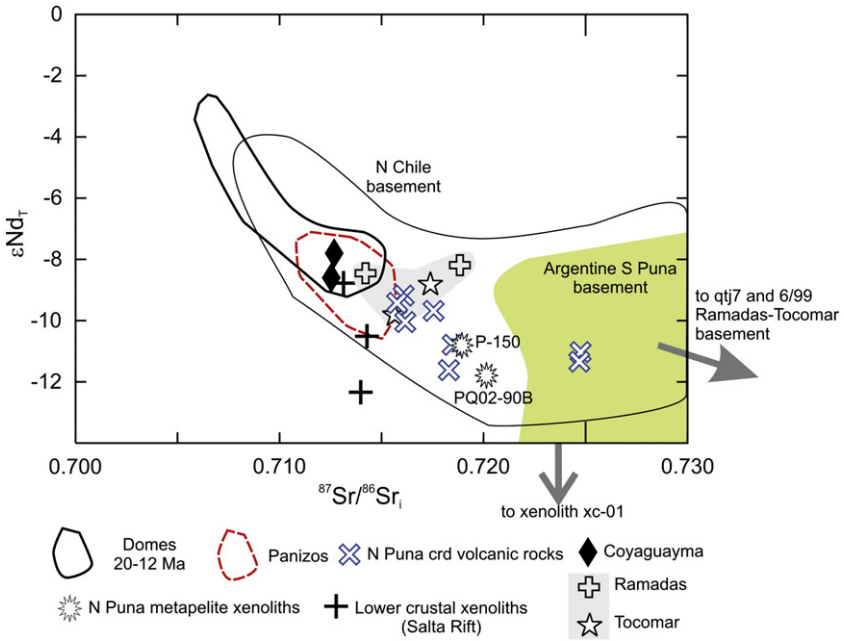

Fig. 11. $^{87}Sr/^{86}Sr_i$ and εNd_T plot for the Coyaguayma ignimbrite pumice and for crustal xenoliths contained in nearby volcanic rocks. Comparison data are shown for 20–12 Ma Puna domes (Caffe et al., 2002), ~7 Ma Panizos ignimbrites and lavas (Ort et al., 1996), 11–10 Ma northern Puna cordierite rhyolites and dacites (authors' unpublished data), 1 Ma Tocomar and 6.6 Ma Ramadas SP rhyolites (Petrinovic et al., 2006; Viramonte et al., 1984, 2007). The $^{87}Sr/^{86}Sr$ and εNd ratios of the lower crustal Salta–Rift granulites, Argentine S Puna and N Chile basement (Lucassen et al., 2001), and metamorphic xenoliths were recalculated to the 11 Ma age of Coyaguayma. Xc-01 is a gneiss xenolith contained in an ignimbrite from Coranzuli caldera (northern Puna); samples qtj7 and 6/99 are basement rocks from the Ramadas–Tocomar area (data from Lucassen et al., 2001).

Table 9
Zircon saturation temperatures.

Sample	Zr (ppm)	M	T_{Zr} (°C)
PQ01-40p	54	1.04	722
PQ04-272p	54	0.90	731
PQ02-97L	51	1.08	715
PQ02-97	72	1.25	730
PQ02-133	88	1.18	751

M = (Na + K + 2Ca) / (Al Si) Molar basis.

feldspar thermometers overlap in the range 690°–730 °C. The mean values for T_{2fsp} are lower than those for T_{GB}, but the two thermometers overlap within the 2σ error (± 50 °C). The T_{2Fsp} results from the Green and Usdansky (1986) model at 5 kbar (~720–730 °C) are closest to the preferred T_{GB} values and are therefore the preferred model temperatures for feldspar crystallization.

8.3. GASP and GBPQ barometers

The GASP barometer is derived from the equilibrium between garnet, Al_2SiO_5, plagioclase and quartz. Like the garnet–biotite thermometer, there are several alternative calibrations for GASP (e.g., Ganguly and Saxena, 1984; Holdaway, 2004; Koziol, 1989; Koziol and Newton, 1988). The Ganguly and Saxena (1984) model is not well-suited for Mn-poor garnet compositions and it yields very low pressures (0.5–1.5 kbar), too low for pressures of magma containing sillimanite as a stable phase. Indeed, if the sillimanite–andalusite equilibrium curve of Richardson et al. (1969) is adopted (cf. Clarke et al., 2005), the stability of sillimanite requires a minimum pressure of ~3–4 kbar for the lowest temperatures estimated by the geothermometry (700–730 °C).

The calibrations of Koziol (1989) and Koziol and Newton (1988) yield more reasonable and consistent pressure values. Based on these and using the average compositions of garnet, plagioclase and biotite, the estimated pressures are 5.4–5.8 kbar (Table 10), with a total range of 4.2 kbar to 6.4 kbar.

Table 10
Garnet–biotite temperatures, for GASP and GBPQ barometers.

Sample PQ01-40p	$P_{GBPQ\ av}$ (kbar)	P_{GASP1} (kbar)	P_{GASP2} (kbar)
	5.0	5.7	5.5
T_{GB} (°C)			
FS 78	779	782	782
HS 82	788	791	790
PG 82	864	865	866
GS 84	883	887	886
Sample PQ02-133	$P_{GBPQ\ av}$ (kbar)	P_{GASP1} (kbar)	P_{GASP2} (kbar)
	5.2	5.8	5.7
T_{GB} (°C)			
FS 78	773	776	775
HS 82	782	785	784
PG 82	858	861	860
GS 84	877	880	880

For sample PQ01-40p: Grt composition is the average of 11 cores; Bt is the average of 16 cores; Pl is the average of 12 cores. For sample PQ02-133: Grt and Bt compositions are the average of 8 cores; Pl is the average of 8 cores. Representative core compositions as in Tables 2, 4 and 5.
FS 78: Ferry and Spear (1978); HS 82: Hodges and Spear (1982); PG 82: Pigage and Greenwood (1982); and GS 84: Ganguly and Saxena (1984).
$P_{GBPQ\ av}$ is the average of Fe- and Mg-rich end-member models of Hoisch (1990). P_{GASP1} and P_{GASP2} are results for the Koziol (1989) and Koziol and Newton (1988) models, considering sillimanite as the stable Al_2SiO_5 phase.
Due to the pressure dependence of T_{GB}, and temperature dependence of P_{GASP} and P_{GBPQ}, solution was obtained simultaneously via iteration, until both estimates concur in a single outcome (see Dahlquist et al., 2007).

Table 11
Two-feldspar temperatures for the Coyaguayma ignimbrite.

	T_{G-U}	T_{F-L}	T_{E-G}	P (kbar)
Sample PQ01-40p				
Pair 1	755	687[a]	695[a]	5
	697	679	686	3
Pair 2	702	666[a]	673	5
	716[a]	657	654	3
Pair 3	687	683	682	5
	649	655	655	3
Pair 4	715	696	674	5
	673	673	661	3
Pair 5	706	676	670	5
	711[a]	659	632[a]	3
Pair 6	719	715	676	5
	656	674	648	3
Pair 7	772	725[a]	712	5
	714	709	690	3
Pair 8	716	693	690	5
	688	680	675	3
Mean ± 2σ (5 kbar)	722 ± 26	693 ± 13	682 ± 14	
Mean ± 2σ (3 kbar)	680 ± 23	673 ± 16	667 ± 15	
Sample PQ02-133				
Pair 1	719	702	689	5
	674	660	649	3
Pair 2	734	700	677	5
	677	682	660	3
Pair 3	752	714	711	5
	684	688	668	3
Pair 4	730	694	687	5
	698	668	657	3
Pair 5	702[a]	710	706	5
	687	630[a]	667	3
Mean ± 2σ (5 kbar)	734 ± 12	704 ± 7	682 ± 16	
Mean ± 2σ (3 kbar)	684 ± 8	675 ± 11	686 ± 19	

All temperatures are in °C.
T_{G-U} Green and Usdansky (1986); T_{F-L} Fuhrman and Lindsley (1988); and T_{E-G} Elkins and Grove (1990).
[a] Data for which Ab, An and/or Or models differ in > 10 °C (excluded from average).

The GBPQ barometer is based in the net transfer reactions between garnet, plagioclase, biotite and quartz (Hoisch, 1990). Mean results obtained for the Fe- and Mg-rich end-member models are 5.0 and 5.2 kbar, respectively (Table 10), with the maximum range between 3.9 and 5.8 kbar. These estimates agree well with those from the GASP barometer and with the constraints on sillimanite stability. We conclude that that the minimum pressure for the equilibrium of the involved phases was ~5 kbar, which is in general agreement with the absence of cordierite in the phenocryst assemblage and with the Mn-poor character of the garnet (Green, 1977; Miller and Stoddard, 1981).

8.5. Pre-eruptive H_2O contents

The pre-eruptive H_2O content was determined following the Putirka (2005) geohygrometer based on melt–plagioclase equilibria. According to the author, the method is most reliable when the temperature of the system is experimentally constrained. However, it seems to yield reasonable results using the empirical temperature estimates for the Coyaguayma ignimbrite. For calculating the H_2O content we used the rim compositions of plagioclase grains (Table 2) that show no signs of disequilibrium with the melt, as represented by analyses of the pumice matrix glass (Table 7).

Using the average two-feldspar T_{G-U} temperatures of 720–730 °C, the calculated pre-eruptive H_2O content in the melt is 7.4–7.6%. These values are slightly higher than the 6.3–6.8% determined from melt inclusions in the metaluminous Toconao rhyolitic ignimbrite (Lindsay et al., 2001). The estimated H_2O contents are consistent with the relationships of SiO_2, crystallinity and wt.% H_2O derived by Scaillet et al. (1998). Based on their analysis, the high crystal content of the Coyaguayma pumice (~30–40% DRE) at 73–75% SiO_2 constrain

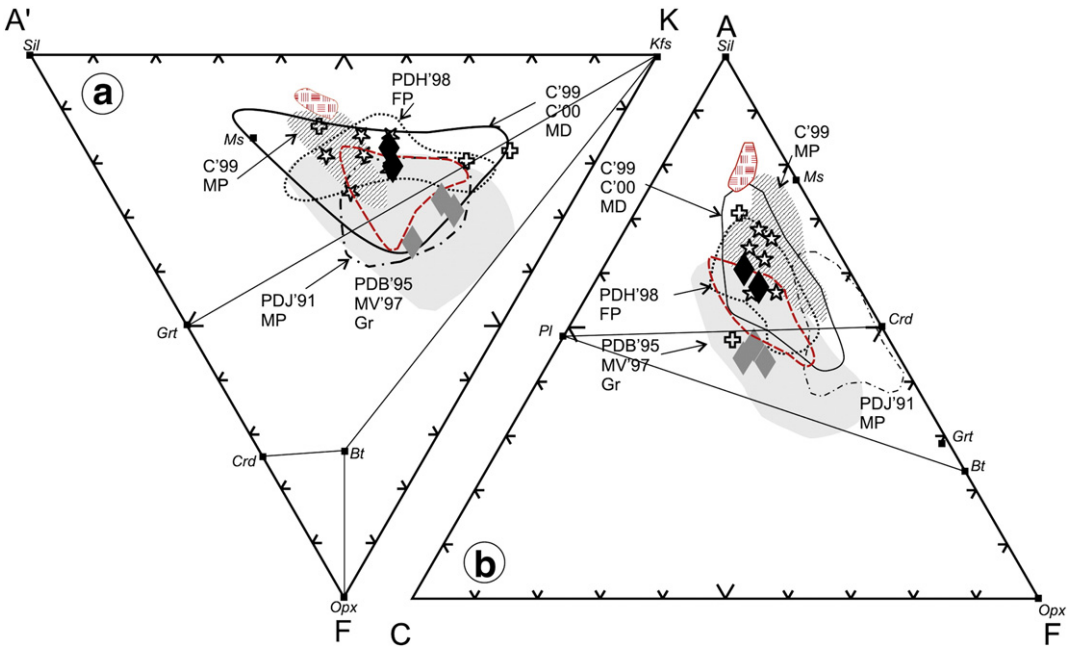

Fig. 13. A′FK and ACF plots for the Coyaguayma ignimbrite pumice and bulk ignimbrite. In A) A′FK: A′ = Al_2O_3–Na_2O–K_2O–CaO; F = FeO_t + MgO; K = K_2O. In B) ACF: A = Al_2O_3–Na_2O–K_2O; C = CaO; F = FeO_t + MgO. All oxides expressed in molar proportions. Bt, Pl, Kfs and Grt represent average compositions of those minerals in the ignimbrite; Ms composition is from Pichavant et al. (1988a); Crd, Sil and Opx are plotted according to stoichiometric Mg-endmember compositions. Fields are shown for experimental melts of metapelites: [PDJ'91 MP, mafic pelite from Patiño Douce and Johnston (1991); PDH'98 FP, felsic pelite from Patiño Douce and Harris (1998); C'99 MP, metapelite from Castro et al. (1999)], metagreywackes [MV'97, from Montel and Vielzeuf (1997); PDB'95, from Patiño Douce and Beard (1995)] and metadacites [C'99; C'00 Md, from Castro et al. (1999, 2000)]. Selected examples of other strongly peraluminous volcanic rocks from the central Andes [Morococala–Macusani andalusite rhyolites; Macusani glasses; Ramadas rhyolite; Tocomar rhyolites] are plotted for comparison, with symbols and references as in Fig. 9.

the pre-eruptive H_2O content to 7–7.2%, in excellent agreement with the Putirka (2005) geohygrometer. It is notable that when both methods are considered, the concentration range for the interstitial melt (7% to 7.6 wt.% H_2O) is well below the saturation level of 8–11 wt.% for the pressures of 4–5 kbar derived from geobarometry (Behrens and Jantos, 2001; Holtz et al., 2001). The Coyaguayma ignimbrite contains 30–40% crystals of mainly anhydrous minerals like quartz, plagioclase and sanidine, so the magmatic H_2O content before crystallization of the major felsic phases was ~4–5%.

9. Discussion

9.1. Origin of the peraluminous minerals

The phenocryst assemblage in the Coyaguayma ignimbrite contains Al_2O_3-rich phases typical of SP rhyolitic magmas. For understanding their significance to magma genesis It is important to establish if these are magmatic, restitic, or xenocrystic in origin (see Clarke, 2007). The petrographic features of sillimanite are ambiguous in terms of their origin (see below), but the habit and textural relations of the garnet and Al-rich biotite suggest that they crystallized from the melt. Garnet and biotite always form individual, euhedral crystals free of reaction rims and almost free of inclusions except for rare microlitic crystals of early accessory phases. Also, garnet and biotite have relatively small sizes, and their low modal proportions are consistent with an origin from an evolved silicic magma. The low Mg# of both phases, low Ti in biotite, and low Mn, Mg and Ca in garnet, as well as the high Al^T and Al^{VI} in biotite are all consistent with a magmatic origin and argue against these phases being xenocrysts or restite minerals. In the case of garnet, the Mn contents are relatively low, in keeping with an origin from highly-evolved silicic melts but the spessartine component is higher than the 10% minimum suggested by Miller and Stoddard (1981) for magmatic garnets in peraluminous magmas (Fig. 8).

Apart from the fact that sillimanite is typically included in other minerals interpreted as magmatic (sanidine, plagioclase, biotite and quartz), it does not show any distinctive textural or compositional features indicative of its origin. A late xenocrystic origin is considered unlikely, partly because metamorphic xenoliths have not been observed in the Coyaguayma ignimbrite, and those that occur in other volcanic rocks from the region (e.g., Corral Negro and Pairique) invariably contain andalusite as the stable Al_2SiO_5 phase (Caffe, unpublished data). Fibrolitic sillimanite was reported in xenoliths from the northern Puna, but in that case it forms distinctive, oriented bundles intergrown with plagioclase, cordierite, corundum, biotite and spinel (Caffe, 1999; Fracchia, 2009). Nothing like that was observed in Coyaguayma. Instead, sillimanite forms well-crystallized prismatic grains as inclusions in early and late phases in the Coyaguayma pumice, and as free crystals in the pumice matrix. This indicates that it was part of the magmatic system for a considerable time; there is no evidence for disequilibrium between the liquid and sillimanite or other phases. Thus, we interpret sillimanite as a restitic or peritectic mineral which remained in equilibrium with the peraluminous melt. This interpretation has consequences for the possible origin of the magma. If the high peraluminosity necessary to stabilize sillimanite was achieved very early, and was acquired at source, two alternative processes can be proposed: a) the rhyolite represents a peraluminous liquid formed by partial melting of crustal rocks (e.g., Pichavant et al., 1988b), or b) it results from extensive assimilation of Al_2O_3-rich country rocks by hot (850–900 °C) intermediate magmas during their emplacement and evolution in the crust (e.g., Lindsay et al., 2001; Pérez-Soba and Villaseca, 2010).

9.2. Genesis of the rhyolite

Key geochemical features of the Coyaguayma ignimbrite pumice for discussing its origin are: high-SiO_2, K_2O/Na_2O, Rb, U, Nb, and Y, and low CaO, CaO/Na_2O, MgO, TiO_2, Sr, Ba, Zr, Th and LREE. These characteristics indicate a geochemically evolved magma, but they

Table 12
Partial melting models of potential protoliths from the Puna basement.

Parents	Rb ppm	Sr ppm	Ba ppm
MAG	123	110	334
MCG	85	220	410
Restite assemblage			
Metapelite Ms melting	Qtz 28 Sil 15 Bt 11 Grt 23 Pl 11K-fsp 11		
Metapelite Ms-Bt melting	Qtz 24 Sil 13 Grt 42 Pl 6K-fsp 14		
Metagreywacke Bt melting	Qtz 15 Opx 40 Grt 10 Pl 35		
Metapelite Ms-vp	Qtz 25 Sil 22 Bt 17 Grt 35		

	Rb/Sr BM	Rb/Sr FM	Rb/Ba BM	Rb/Ba FM
MAG Ms melt 1 (11%)	3.7	3.91	1.23	1.92
MAG Ms melt 2 (11%)	3.6	4.75	3.58	3.12
MAG Ms vp melt 1 (40%)	0.6	1.05	0.6	1.84
MAG Ms vp melt 2 (20%)	0.68	1.3	1.72	2.57
MAG Ms–Bt melt 1 (30%)	4.94	8.27	1.14	3.4
MAG Ms–Bt melt 2 (30%)	3.91	5.59	1.93	3.67
MCG Bt melt 1 (50%)	1.15		0.24	
MCG Bt melt 2 (50%)	2.09		0.44	
MCG Bt melt 3 (40%)	1.52		0.25	
MCG Bt melt 4 (40%)	2.90		0.54	

MAG: Mean Argentine Puna gneiss (metapelite) and MCG: Mean N Chilean gneiss (metagreywacke). Data from Lucassen et al. (1999). BM: Batch Melting and FM: Fractional Melting. All models following the equations of Hanson (1978). Vp is vapor present melting, the rest are vapor absent. Numbers in parenthesis are degree of melting in each case.
For metapelitic sources Ms dehydration melting reaction considered is Ms (Fe- and Mg-rich, F-poor) + Pl + Qtz = Melt + K-fsp + Sil + Bt (Patiño Douce and Harris, 1998), whereas Bt dehydration melting takes the form of Pl + Bt + Sil + Qtz = Melt + Grt + K-fsp (Vielzeuf and Holloway, 1988). Reactions are thought to occur at T > 800–900 °C and P = 6–10 kbar (Patiño Douce and Harris, 1998). Melt productivity (~10–32%) is similar to those presented by Harris and Inger (1992).
For metagreywacke protoliths, the modeled Bt dehydration melting reaction is Bt + Qtz + Pl = Melt + Opx + K-fsp + Grt (Montel and Vielzeuf, 1997; Patiño Douce and Beard, 1995; Vielzeuf and Montel, 1994), occurring at T > 800° to 1000 °C and P > 4 to 12 kbar, with a melt productivity of (40–50%).

are not diagnostic of any specific mechanism of magma genesis and evolution. Such compositions may be produced either by direct partial melting of metasediments, or by fractionation of crustally contaminated dacitic magmas. In this section, the pros and cons of both petrogenetic interpretations are discussed.

9.2.1. Mica dehydration melting

The most convincing evidence supporting an origin of the Coyaguayma ignimbrite by partial melting of crustal protholiths is the strongly peraluminous nature of the pumice, and its compositional coincidence (Fig. 13) with experimental dehydration melts of metagreywackes and felsic metapelites (Castro et al., 1999, 2000; Montel and Vielzeuf, 1997; Patiño Douce and Harris, 1998).

The abundances of Rb, Ba and Sr are controlled by the mineralogy of the source during melting, and their contents are consistent with an origin by melting of mica-bearing rocks under vapor-absent conditions (Harris and Inger, 1992; Sylvester, 1998). Also, muscovite and biotite dehydration-melting reactions would be possible at the temperatures and pressures slightly above the maximum estimated crystallization conditions of the Coyaguayma magma (ca. 800 °C at 5 kbar). Therefore, the melting hypothesis was tested by calculating model Sr, Ba and Rb concentrations (Table 12) for batch and fractional melting (Hanson, 1978) of average Chilean (metagreywacke) and Argentine (metapelitic) gneisses using data from Lucassen et al. (1999, 2001). The geochemical models which best reproduce the composition of the Coyaguayma pumice (Fig. 14) and also satisfy the thermobarometric constraints (details of partial melting reactions, melt productivity and restite mineralogy are in Table 12), result from fractional melting of average Argentine Puna gneiss. Chilean gneisses as a source rock produce melts with lower Rb/Ba and Rb/Sr than observed, but coincident with some of the cordierite-bearing volcanic rocks from the broader region (Fig. 14). However, we note that the melting model cannot explain the high Rb/Sr and Rb/Ba ratios of the Tocomar and Ramadas rhyolites (Fig. 14). These compositions would require further crystal fractionation, similar to the suggestion by Pichavant et al. (1987) for the Macusani glasses, which have even higher Rb/Sr and Rb/Ba ratios.

The pure melting scenario is consistent with observed Rb, Sr and Ba contents but it has two main problems. First is the very low

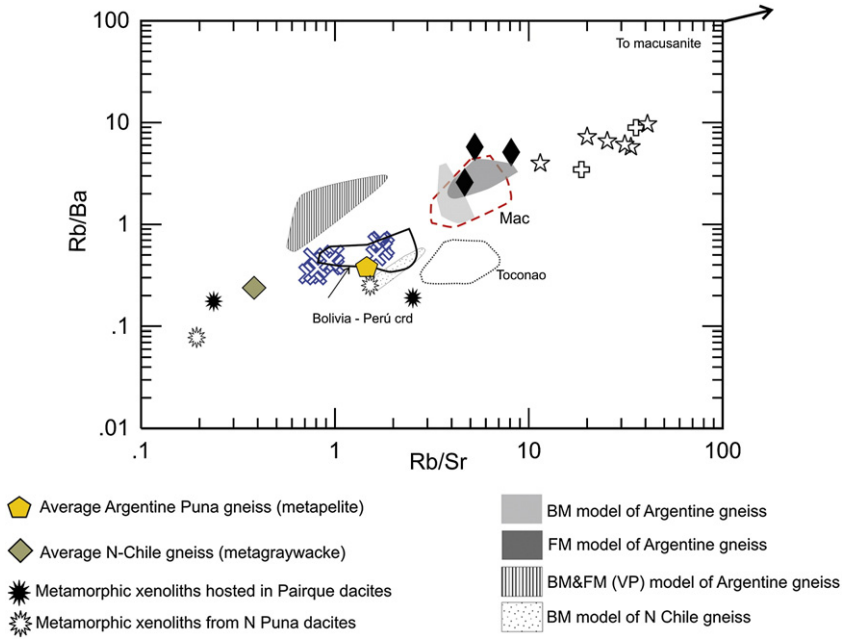

Fig. 14. Plot of Rb/Ba versus Rb/Sr ratios calculated for vapor-absent batch (BM) and fractional (FM) melting models of average Argentine Puna and N Chile gneisses (Table 13). Vapor-present (VP) melts and Coyaguayma pumice composition are shown. Also plotted for comparison are xenoliths in the Pairique volcanic complex and other N Puna volcanic centers (authors' unpublished data), N Puna cordierite rhyolites and dacites (open crosses), the metaluminous Toconao rhyolite, and other SP rhyolites (Macusani, Tocomar and Ramadas). Symbols and references as in Fig. 9.

Table 13
Contamination and crystal fractionation model for the Coyaguayma pumice.

Mixing model

0.7 Atana crystal rich pumice + 0.3 Morococala (andalusite rhyolite) SP melt

	SiO2	TiO2	Al2O3	FeOt	MnO	MgO	CaO	Na2O	K2O	P2O5	Rb	Ba	Sr	Y	$^{87}Sr/^{86}Sr$
Atana	68.0	0.51	15.0	2.75	0.06	1.08	3.02	2.91	4.10	0.13	195	585	247	26	0.710
SP melt	73.5	0.14	14.7	0.97	0.02	0.26	0.77	2.60	4.85	0.28	479	330	130	10	0.725
Mix	69.7	0.40	14.91	2.22	0.05	0.83	2.35	2.82	4.34	0.18	280	508	212	21	0.713

Fractionation LSQ model

Coef	%Solid	Mineral separated
0.254	35.9	Plagioclase (Loy 97-h-2)
0.202	28.6	Quartz
0.175	24.7	Sanidine (PQ01-40p)
0.007	1.0	Magnetite (Loy-97-h-2)
0.065	9.1	Biotite (Loy-97-h-2)
0.005	0.6	Apatite (PQ01-25)

F = 0.293
Major elements (wt.%)

	Daughter	Obs. par.	Calc. par.	Differ.	LSQr
	PQ01-40p[a]	Mix[a]			
SiO_2	75.36	71.28	71.26	0.01	0.025
TiO_2	0.05	0.41	0.37	0.04	
Al_2O_3	14.77	15.25	15.21	0.04	
FeOt	1.18	2.27	2.27	0.00	
MnO	0.06	0.05	0.04	0.01	
MgO	0.10	0.85	0.87	−0.03	
CaO	0.77	2.40	2.35	0.05	
Na_2O	2.44	2.88	3.01	−0.12	
K_2O	5.09	4.43	4.43	0.00	
P_2O_5	0.17	0.18	0.25	−0.06	

Trace elements (ppm)

	Pq01-40p	Cl (Eq)	Cl (Ray)	Parent	D	(F = 0.293)
Rb	350	351	451	280	0.78	
Ba	64	62	0	508	9.65	
Sr	50	36	0	212	6.56	
Y	30	33	49	21	0.17	

Atana crystal rich pumice is Lari-96h-6 (Lindsay et al., 2001), SP melt is the Andalusite rhyolite Mor 85-18 (Morgan et al., 1998) assuming the same $^{87}Sr/^{86}Sr$ as the Macusani ignimbrites (Pichavant et al., 1988b). Minerals from Lindsay et al. (2001), except for K-fsp (type-b sanidine; this work) and apatite (from Caffe and Trumbull, 2006). Mix is the hypothetical hybrid parent before fractionation. F is the remaining liquid after fractionation. LSQr is the sum of squares of residuals. Equilibrium [Cl(Eq.)] and Rayleigh [Cl (Ray)] fractionation models according to equation in Rollinson (1993). Kds for all minerals from Nash and Crecraft (1985) except for Y in apatite (Pearce and Norry, 1979).
[a] Oxides recalculated to 100%, anhydrous basis.

concentration of Th, Zr and LREE of the Coyaguayma pumice, a characteristic that is common to all of the Puna SP rhyolites. This could possibly be explained by disequilibrium partial melting that prevents these elements in the source from entering the melt (i.e., rapid melting and/or segregation before complete dissolution of accessory phases; Villaros et al., 2009), or retention of these elements in high-pressure residual minerals (Villaseca et al., 2007). However, the observed relatively low HREE slopes of the Coyaguayma ignimbrite pumice preclude the latter hypothesis, whereas low $^{87}Sr/^{86}Sr_i$ ratios (see below) contradicts the former, since disequilibrium mica-dehydration melting would produce high Rb/Sr melts with higher $^{87}Sr/^{86}Sr$ than the source rocks, which is opposite to what is observed (Zeng et al., 2005).

Second and most important, the low $^{87}Sr/^{86}Sr_i$ ratios (~0.7125) of the Coyaguayma ignimbrite, and of other SP rhyolites Tocomar ($^{87}Sr/^{86}Sr_i$ 0.715–0.717) and Ramadas ($^{87}Sr/^{86}Sr_i$ 0.714–0.719) do not match those of the exposed basement or of crustal xenoliths hosted in northern Puna volcanic rocks (Fig. 11). A possible explanation for the low $^{87}Sr/^{86}Sr_i$ ratios would be melting of deeper, crustal rocks of higher grade with less radiogenic Sr (i.e., lower time-integrated Rb/Sr ratio) than the outcropping basement. Possible candidates are the lower crustal felsic granulite xenoliths from the Salta Rift basanites (Fig. 11). However, partial melting of granulite-facies rocks would require very high temperatures (>950–1000 °C) and/or a previous hydration of the source, and from experimental evidence, is likely to produce melts with lower Rb/Sr and less Al_2O_3-rich [A/CNK <1.2; $Al_2O_3/(MgO + FeO) \leq 4$; Patiño Douce and Beard, 1995] than the Coyaguayma pumice, or melts that are trondhjemitic in composition (Patiño Douce and Harris, 1998). Moreover, the $^{206}Pb/^{204}Pb_{11Ma}$ ratios of lower crustal xenoliths do not match those in the Coyaguayma ignimbrite (Fig. 12). Another alternative is to invoke the participation of fertile (mid- or upper crustal) sources with lower $^{87}Sr/^{86}Sr_i$ ratios than the exposed basement, but this is not supported by any currently available data for xenoliths in the region. We therefore conclude that the Coyaguayma magma did not originate by partial melting of crustal sources alone.

9.2.2. Crystal fractionation of hybrid magmas

As described above, strong arguments against pure crustal melting are the low contents of trace elements (Sr, Ba, Zr, Th and LREE) that are compatible in the Coyaguayma mineral assemblage (plagioclase, sanidine, monazite and zircon) and, especially, the low initial $^{87}Sr/^{86}Sr$ ratios observed in the Coyaguayma ignimbrite ($^{87}Sr/^{86}Sr_i$ ~0.7125) compared with probable source rocks in the pre-Cenozoic basement. These initial Sr isotope ratios are in the lower range of calc-alkaline ignimbrites and lavas (Panizos, Lower Miocene volcanic domes) from

northern Puna (Table 8 and Fig. 11) that are considered to represent approximate 50–50 mixtures of crustal and mantle magmas (Caffe et al., 2002; Kay et al., 2010a). The isotopic compositions of the Coyaguayma ignimbrite can be readily explained by mixing 30% crustal melts derived from metapelites (similar to andalusite-bearing rhyolites from Bolivia and Perú), and 70% of typical central Andean calc-alkaline dacitic magma (similar to the Atana ignimbrite, Table 13). The major and trace element composition of this mixture differs from that of Coyaguayma pumice, but the differences can be explained by subsequent fractionation without a change in isotope ratios. Least squares modeling (Table 13) suggests that the major and trace element composition of the Coyaguayma pumice can be achieved after about 70% equilibrium fractional crystallization of plagioclase, quartz, sanidine (Ba-rich), biotite, magnetite and apatite from the hybrid starting magma (LSQ residuals of 0.025). The low observed contents of Zr, Th and LREE require very small (≤0.1%) removal of monazite and zircon (by inclusion of these minerals in fractionating silicates). It is noted that the sequential mechanism of forming a hybrid magma by mixing/assimilation followed by closed-system fractionation yields better results than combined assimilation and fractional crystallization (AFC; De Paolo, 1981). In conventional AFC modeling, the observed $^{87}Sr/^{86}Sr$ ratios and Sr and Ba concentrations are reached by addition of just 15% (F = 0.85 for r ~ 0.5) of crustal assimilants, whereas the Rb concentrations, and more importantly, those of most major elements as well as the A/CNK ratios, would require a large amount of additional, plagioclase-dominated fractionation and this in turn would depress the Ba and Sr concentrations below the observed values.

To summarize, the scenario suggested by the arguments above and consistent with geochemical modeling is a two-phase evolution. Hot calc-alkaline dacite magma, whose main geochemical and isotopic characteristics were acquired by AFC processes in the lower crust (e.g., Kay et al., 2010a), ascends and accumulates in the middle crust where it encounters fertile metapelite rocks. The mid-crustal magma accumulation may relate to the zone of partial melting under the Puna–Altiplano plateau that is imaged by geophysics (see review in Schilling et al., 2006). Crustal contamination likely proceeded by partial melting of the metapelite country rocks and mixing with the derived melt. Partial melting reactions in metapelites typically produce peraluminous phases like cordierite/garnet and aluminosilicates, and entrainment of this restitic/peritectic material possibly took place during melt segregation to explain the presence of sillimanite. Contamination of the dacitic magma by SP partial melts was followed by extensive fractionation before ascent of the residual melt to a shallow crustal magma chamber (T = <800 °C and P = ~4–5 kbar). There, additional crystallization (without fractionation) took place before eruption of the crystal-rich SP rhyolite represented by the Coyaguayma ignimbrite.

Contamination in this model is envisaged as mainly mixing of the hot, dacitic magma with a melt derived from the mid-crustal country rocks. An alternative and closely related mechanism, suggested by Beard et al. (2005) and Díaz-Alvarado et al. (2011), is reactive bulk assimilation whereby solid fragments of metapelite are entrained in the dacite magma and undergo thermal and mechanical disintegration. The latter process offers an efficient way to transport restitic or peritectic phases into the bulk magma and this can cause a deviation of magma compositions from the expected cotectic fractionation trends (Díaz-Alvarado et al., 2011). We see no evidence for reactive bulk assimilation in the Coyaguayma rhyolite. Bulk-rock compositions follow geochemical trends expected for fractional crystallization of a felsic magma and there are no metapelitic xenoliths in the ignimbrite. Nevertheless, these observations do not necessarily rule out reactive bulk assimilation because in the two-stage scenario the mid-crustal assimilation is followed by extensive fractional crystallization of the hybrid magma that would mask the geochemical effects of assimilation. Whatever the exact process of assimilation was, sillimanite may be considered a witness of the contamination process, if as is likely, it formed as a product of the dehydration melting reactions. The survival of sillimanite throughout the subsequent magma fractionation and ascent is consistent with studies (Erdmann et al., 2004, 2007; Díaz-Alvarado et al., 2011; and references therein) showing that peraluminous minerals (e.g., cordierite; sillimanite) produced during reactive assimilation survive in local equilibrium with the hybrid magma. Indeed, sillimanite is stable in hydrous (4–8 wt.% H_2O) leucogranite melts with A/CNK ratios of 1.15–1.30 and T = 700–800 °C (Acosta-Vigil et al., 2003), conditions appropriate for the Coyaguayma magma.

The other SP SiO_2-rich rhyolites from the northern Puna (Tocomar and Ramadas) share most of the chemical (Al_2O_3- and SiO_2-rich nature, low Sr, Ba, Th and LREE) and isotopic characteristics of the Coyaguayma ignimbrite (Fig. 11), suggesting similar petrogenesis of these occurrences in the central Andes plateau. In contrast to Coyaguayma, these units are almost aphyric, which reinforces the idea of an origin from residual melts after fractionation of hybrid SP magmas. There are, however, some differences between the Coyaguayma ignimbrite and other Puna SP rhyolites that suggest local variations in the general model. For example, slightly higher initial $^{87}Sr/^{86}Sr$ ratio and Rb concentration in Tocomar and Ramadas rhyolites suggest higher contents of the metapelitic contaminant, whereas their lower Sr and Ba contents, as well as larger negative Eu anomalies imply larger amounts of feldspar-dominated fractionation after assimilation.

10. Concluding remarks

The Coyaguayma ignimbrite is a SiO_2-rich SP rhyolite with major (high A/CNK and K_2O, low CaO, Ti, FeO and MgO) and trace element (low Ba, Sr, Zr, Th, LREE and Eu/Eu*; high HREE, Y, Rb, Nb and U) composition, as well as petrological characteristics (e.g., a stable Al_2O_3-rich mineralogy; crystallization range of 800–720 °C at 4–5 kbar; initial H_2O contents of ~4–5%) that are similar to many S-type leucogranites. The latter have generally been considered as the direct products of dehydration partial melting of metapelite sources (e.g., Patiño Douce and Harris, 1998; Sylvester, 1998). However, in the case of Coyaguayma these geochemical features, combined with the relatively low $^{87}Sr/^{86}Sr_i$ (~0.7125), and high $^{143}Nd/^{144}Nd_i$ (0.512220) and $^{206}Pb/^{204}Pb_i$ (18.85) ratios are inconsistent with an origin by melting of pre-Cenozoic basement lithologies from the central Andes. The observed compositions can be modeled successfully by a two-stage process involving crustal contamination of calc-alkaline dacite magmas typical for the large-volume APVC ignimbrites (e.g., Atana) followed by extensive crystal fractionation of the derived magma. Geochemical modeling suggests mixing of dacitic magma with ~30% partial melts of metapelitic country rocks in mid-crustal depths (>5–6 kbar), and subsequent fractionation (70%) of plagioclase, quartz, K-feldspar, biotite, minor apatite and magnetite, and traces of zircon and monazite. Sillimanite in the ryholite is interpreted as restitic or a product of incongruent partial melting reactions in the contaminant.

Afterwards, the Coyaguayma magma ascended and underwent further crystallization of minor almandine-spessartine garnet and Al-rich biotite (early cotectic phases), and larger amounts (~30%) of oligoclase, quartz, and Ba-poor sanidine (main cotectic phases). The latter magmatic stage occurred at 4–5 kbar and ~800 °C to 720 °C, just before explosive eruption.

The petrogenetic model presented here can be applied with minor variations to the other rare occurrences of SiO_2-rich SP volcanic rocks from the Puna plateau region, such as the Tocomar and Ramadas rhyolites. In addition, this model may be more widely applicable than simple dehydration partial melting to explain leucogranitic SP igneous rocks in continental arc settings.

Acknowledgments

We want to thank Miguel Soler, Liza Polo and Agustín Cabrera who helped us during field work. Betty Coira, Eduardo Medina and Dieter

Rhede graciously permitted access to the XRF, SEM and Electron Microprobe laboratories at the Instituto de Geología y Minería (UNJu), Universidad Católica del Norte (Antofagasta) and GFZ Potsdam, respectively. Roberto Liquin, Paulino Cachizumba and Patrocinio Flores (Jujuy), as well as Oona Appelt, Gerhard Berger (Potsdam), and Elmar Reitter (Tübingen), generously helped us during whole-rock XRF, EMP mineral and isotope analyses. This paper largely benefited from discussions on granite and rhyolite genesis with Betty Coira, Diego Fracchia, Javier Elortegui, José M. Viramonte, Raul Becchio and Alfonso Sola, some of whom facilitated unpublished geochemical data for comparison. The insightful comments of Antonio Castro and an anonimous reviewer largely improved the quality of the original manuscript. Financial aid came from grants ANPCyT7-12376 and 7-38131, CONICET PIP 2010 No. 204 and SeCTER-UNJu08/E028. Pablo Caffe is indebted to DAAD for supporting a postdoctoral visit to the GFZ Potsdam in 2004.

References

Abdel-Rahman, A.M., 1994. Nature of biotites from alkaline, calc-alkaline and peraluminous magmas. Journal of Petrology 35, 525–541.

Acosta-Vigil, A., London, D., Morgan, G.B., Dewers, T.A., 2003. Solubility of excess alumina in hydrous granitic melts in equilibrium with peraluminous minerals at 700–800ºC and 200MPa, and applications of the aluminum saturation index. Contributions to Mineralogy and Petrology 146, 100–119.

Anderson, J.L., 1996. Status of thermobarometry in granitic batholiths. Transactions of the Royal Society of Edinburgh Earth Sciences 87, 125–138.

Bea, F., 1996. Residence of REE, Y, Th and U in granites and crustal protoliths; implications for the chemistry of crustal melts. Journal of Petrology 37, 521–552.

Beard, J.S., Ragland, P.C., Crawford, M.L., 2005. Reactive bulk assimilation: a model for crust–mantle mixing in silicic magmas. Geology 33, 681–684.

Behrens, H., Jantos, N., 2001. The effect of anhydrous composition on water solubility in granitic melts. American Mineralogist 86, 14–20.

Birck, J.L., 1986. Precision K–Rb–Sr isotopic analyses application to Rb–Sr chronology. Chemical Geology 56, 73–83.

Caffe, P.J., 1999. Complejos volcánicos dómicos del Terciario superior de Puna Norte: sus implicancias magmatotectónicas y metalogenéticas. PhD Thesis (unpublished). Facultad de Ciencias Exactas, Físicas y Naturales, Universidad Nacional de Córdoba, Argentina, 421 pp.

Caffe, P.J., Trumbull, R.B., 2006. The Pairique cordierite–biotite dacites: a clue to the petrogenesis of peraluminous magmas in the APVC region. Backbone of the Americas, Abstract with Programs No. 2, p. 33 (Mendoza).

Caffe, P.J., Trumbull, R.B., Coira, B.L., Romer, R.L., 2002. Petrogenesis of Early Neogene magmatism in the northern Puna; implications for magma genesis and crustal processes in the Central Andean Plateau. Journal of Petrology 43, 907–942.

Caffe, P.J., Soler, M.M., Rodriguez, G., Coira, B., Onoe, A.T., 2005. El Complejo Volcánico Pairique. Volcanismo peraluminoso tipo S en los Andes Centrales del Sur. : Actas del XVI Congreso Geológico Argentino, Tomo, 1. La Plata, pp. 643–650.

Caffe, P.J., Soler, M.M., Coira, B., Cabrera, A., Flores, P., 2007. Estratigrafía y centros eruptivos de la región de Pairique, Puna Jujena. Revista Asociación Geológica Argentina 62, 242–246.

Castro, A., Patiño Douce, A.E., Corretgé, L.G., De La Rosa, J.D., El-Biad, M., El-Hmidi, H., 1999. Origin of peraluminous granites and granodiorites, Iberian massif, Spain. An experimental test of granite petrogenesis. Contributions to Mineralogy and Petrology 135, 255–276.

Castro, A., Corretgé, L.G., El-Biad, M., El-Hmidi, H., Fernández Rodríguez, C., Patiño Douce, A., 2000. Experimental constraints on Hercynian anatexis in the Iberian Massif, Spain. Journal of Petrology 41, 1471–1488.

Chappell, B.W., White, A.J.R., 2001. Two contrasting granite types: 25 years later. Australian Journal of Earth Sciences 48, 489–499.

Clarke, D.B., 1981. The mineralogy of peraluminous granites: a review. The Canadian Mineralogist 19, 3–17.

Clarke, D.B., 2007. Assimilation of xenocrysts in granitic magmas; principles, processes, proxies, and problems. The Canadian Mineralogist 45, 5–30.

Clarke, D.B., Dorais, M., Barbarin, B., Barker, D., Cesare, B., Clarke, G., el Baghdadi, M., Erdmann, S., Förster, H.-J., Gaeta, M., Gottesmann, B., Jamieson, R.A., Kontak, D.J., Koller, F., Gomes, C.L., London, D., Morgan VI, G.B., Neves, L.J.P.F., Pattison, D.R.M., Pereira, A.J.S.C., Pichavant, M., Rapela, C., Renno, A.D., Richards, S., Roberts, M., Rottura, A., Saavedra, J., Sial, A.N., Toselli, A.J., Ugidos, J.M., Uher, P., Villaseca, C., Visonà, D., Whitney, D.L., Williamson, B., Woodard, H.H., 2005. Occurrence and origin of andalusite in peraluminous felsic igneous rocks. Journal of Petrology 46, 441–472.

Clemens, J.D., Wall, V.J., 1984. Origin and evolution of a peraluminous silicic ignimbrite suite: the Violet Town Volcanics. Contributions to Mineralogy and Petrology 88, 354–371.

Coira, B., Caffe, P.J., Kay, S.M., Díaz, A., Ramirez, A., 1996. Complejo volcánico Vilama - Sistema caldérico del Cenozoico superior en Puna, Jujuy. XIII Congreso Argentino de Geología, Actas 3, 603–620. Buenos Aires.

Coira, B., Caffe, P.J., Ramírez, A., Chayle, W., Díaz, A., Rosas, S.A., Pérez, A., Pérez, E.M.B., Orosco, O., Martínez, M., 2004. Hoja Geológica 2366-I Mina Pirquitas (1:250.000). SEGEMAR Secretaría de Minería de la Nación: Boletín, 269, pp. 1–123.

Collins, B.W., 1996. Lachlan fold belt granitoids; products of three-component mixing. In: Brown, M., Candela, P.A., Peck, D.L., Stephens, W.E., Walker, R.J., Zen, E-an (Eds.), Third Hutton Symposium on the Origin of Granites and Related Rocks: Geological Society of America, Special Papers, 315, pp. 171–181.

Crock, J.G., Lichte, F.E., Wildeman, T.R., 1984. The group separation of the rare-earth elements and yttrium from geologic materials by cation-exchange chromatography. Chemical Geology 45, 149–163.

Dahlquist, J.A., Rapela, C.W., Baldo, E.G., 2005. Petrogenesis of cordierite-bearing S-type granitoids in Sierra de Chepes, Famatinian orogen, Argentina. Journal of South American Earth Sciences 20, 231–251.

Dahlquist, J.A., Galindo, C., Pankhurst, R.J., Rapela, C.W., Alasino, P.H., Saavedra, J., Fanning, C.M., 2007. Magmatic evolution of the Peñón Rosado granite: petrogenesis of garnet-bearing granitoids. Lithos 95, 177–207.

De Paolo, D.J., 1981. Trace element and isotopic effects of combined wallrock assimilation and fractional crystallization. Earth and Planetary Science Letters 53, 189–202.

de Silva, S.L., 1989. The Altiplano–Puna volcanic complex of the central Andes. Geology 17, 1102–1106.

Díaz-Alvarado, J., Castro, A., Fernández, C., Moreno-Ventas, I., 2011. Assessing bulk assimilation in cordierite-bearing granitoids from the Central System Batholith, Spain; experimental, geochemical and geochronological constraints. Journal of Petrology 56, 223–256.

Droop, G.T.R., 1987. A general equation for estimating Fe^{3+} concentrations in ferromagnesian silicates and oxides from microprobe analyses, using stoichiometric criteria. Mineralogical Magazine 51, 431–435.

Elburg, M.A., 1996. Genetic significance of multiple enclave types in a peraluminous ignimbrite suite, Lachlan Fold Belt, Australia. Journal of Petrology 37, 1385–1408.

Elkins, L.T., Grove, T.L., 1990. Ternary feldspar experiments and thermodynamic models. American Mineralogist 75, 544–559.

Elortegui Palacios, J., Caffe, P.J., Coira, B., 2011. Fusión parcial y desmezcla restítica vinculada al origen de dos asociaciones magmáticas graníticas ordovícicas de la Puna jujeña. Actas del XVIII Congreso Geológico Argentino, Neuquén (CD-ROM).

Erdmann, S., Clarke, D.B., MacDonald, M.A., 2004. Origin of chemically zoned and unzoned cordierites from the South Mountain and Musquodoboit batholiths. Transactions of the Royal Society of Edinburgh Earth Sciences 95, 99–110.

Erdmann, S., London, D., Morgan VI, G.B., Clarke, B.D., 2007. The contamination of granitic magma by metasedimentary country-rock material: an experimental study. The Canadian Mineralogist 45, 43–61.

Ferry, J.M., Spear, F.S., 1978. Experimental calibration of partitioning Fe and Mg between biotite and garnet. Contributions to Mineralogy and Petrology 66, 113–117.

Fracchia, D., 2009. Volcanismo postcolapso de la Caldera Vilama, Mioceno superior, Puna argentino–boliviana: Mecanismos eruptivos y Petrogénesis. Ph.D. Thesis (unpublished). Facultad de Ciencias Naturales y Museo, Universidad Nacional de la Plata, Argentina. 459 pp.

Fuhrman, M.L., Lindsley, D.L., 1988. Ternary-feldspar modeling and thermometry. American Mineralogist 73, 201–215.

Ganguly, J., Saxena, S., 1984. Mixing properties of aluminosilicate garnets: constraints from natural and experimental data, and applications to geothermo-barometry. American Mineralogist 69, 88–97.

Gauthier, J.P., Deruelle, B., Viramonte, J.G., Aparicio, A., 1994. Grenats des rhyolites de la caldera de La Pava — Ramadas (NW Argentine) et de leurs xenolites granitiques. Comptes Rendus de l'Académie des Sciences de Paris, Série II, 318, pp. 1629–1635.

Gerstenberger, H., Haase, G., 1997. A highly effective emitter substance for mass spectrometric Pb isotope ratio determinations. Chemical Geology 136, 309–312.

Goldstein, S.L., O'Nions, R.K., Hamilton, P.J., 1984. A Sm–Nd study of atmospheric dusts and particulates from major river systems. Earth and Planetary Science Letters 70, 221–236.

Green, T.H., 1977. Garnet in silicic liquids and its possible use as a P–T indicator. Contributions to Mineralogy and Petrology 65, 59–67.

Green, N.L., Usdansky, S.I., 1986. Ternary feldspar mixing relations and thermobarometry. American Mineralogist 71, 1100–1108.

Guzmán, S., Petrinovic, I.A., Brod, J.A., Hongn, F.D., Seggiaro, R.E., Montero, C., Carniel, R., Dantas, E.L., Sudo, M., 2011. Petrology of the Luingo caldera (SE margin of the Puna plateau): a middle Miocene window of the arc–back arc configuration. Journal of Volcanology and Geothermal Research 200, 171–191.

Hanson, G.N., 1978. The application of trace elements to the petrogenesis of igneous rocks of granitic composition. Earth and Planetary Science Letters 38, 26–43.

Harangi, S., Downes, H., Kosa, L., Szabo, C., Thirlwall, M.F., Mason, P.R.D., Mattey, D., 2001. Almandine garnet in calc-alkaline volcanic rocks of the Northern Pannonian Basin (Eastern-Central Europe): geochemistry, petrogenesis and geodynamic implications. Journal of Petrology 42, 1813–1843.

Harris, N.B.W., Inger, S., 1992. Trace element modeling of pelite-derived granites. Contributions to Mineralogy and Petrology 110, 46–56.

Hodges, K.V., Spear, F.S., 1982. Geothermometry, geobarometry and the Al_2SiO_5 triple point at Mt. Moosilauke, New Hampshire. American Mineralogist 67, 1118–1134.

Hoisch, T.D., 1990. Empirical calibration of six geobarometers for the mineral assemblage quartz + muscovite + biotite + plagioclase + garnet. Contributions to Mineralogy and Petrology 104, 225–234.

Holdaway, M.J., 2000. Application of new experimental and garnet Margules data to the garnet–biotite geothermometer. American Mineralogist 85, 881–892.

Holdaway, M.J., 2004. Optimization of some key geothermobarometers for pelitic metamorphic rocks. Mineralogical Magazine 68, 1–14.

Holtz, F., Johannes, W., Tamic, N., Behrens, H., 2001. Maximum and minimum water contents of granitic melts generated in the crust: a reevaluation and implications. Lithos 56, 1–14.

Jacobsen, K., Wasserburg, G.J., 1980. Sm–Nd isotopic evolution of chondrites. Earth and Planetary Science Letters 50, 139–155.

Kaneko, Y., Miyano, T., 2004. Recalibration of mutually consistent garnet–biotite and garnet–cordierite geothermometers. Lithos 73, 255–269.

Kay, S.M., Coira, B., Caffe, P.J., Chen, C.-H., 2010a. Regional chemical diversity, crustal and mantle sources and evolution of central Andean Puna Plateau Ignimbrites. Journal of Volcanology and Geothermal Research 198, 81–111.

Kay, S.M., Keller, C.B., Coira, B., Jiménez, N., Caffe, P.J., 2010b. Chemistry of post-12 Ma Los Frailes Volcanic Complex ignimbrites in Bolivia and the role of magmatism in the uplift of the Central Andean Altiplano Plateau. American Geophysical Union, Fall Meeting 2010, San Francisco (Abstract #T13D-08).

Kontak, D.J., Clark, A.H., 1997. The Minastira peraluminous granite, Puno, southeastern Peru; a quenched, hypabyssal intrusion recording magma commingling and mixing. Mineralogical Magazine 61, 743–764.

Koziol, A.M., 1989. Recalibration of the garnet–plagioclase–Al_2SiO_5–quartz (GASP) geobarometer and applications to natural paragenesis. Eos 70, 493.

Koziol, A.M., Newton, R.C., 1988. Grossular activity–composition relations in ternary garnets determined by reversed displaced-equilibrium experiments. Contributions to Mineralogy and Petrology 103, 423–433.

Kretz, R., 1983. Symbols for rock-forming minerals. American Mineralogist 68, 277–279.

Kroll, H., Evangelakakis, C., Voll, G., 1993. Two-feldspar geothermometry: a review and revision for slowly cooled rocks. Contributions to Mineralogy and Petrology 114, 510–518.

Lindsay, J.M., Schmitt, A.K., Trumbull, R.B., de Silva, S.L., Siebel, W., Emmermann, R., 2001. Magmatic evolution of the La Pacana caldera system, Central Andes, Chile: compositional variation of two cogenetic, large-volume felsic ignimbrites. Journal of Petrology 42, 459–486.

Lucassen, F., Franz, G., Thirlwall, M.F., Mezger, K., 1999. Crustal recycling of metamorphic basement: Late Paleozoic granitoids of northern Chile (22°S). Implications for the composition of the Andean crust. Journal of Petrology 40, 1527–1551.

Lucassen, F., Becchio, R., Harmon, R., Kasemann, S., Franz, G., Trumbull, R., Wilke, H.-G., Romer, R.L., Dulski, P., 2001. Composition and density model of the continental crust at an active continental margin — the central Andes between 21° and 27° S. Tectonophysics 341, 195–223.

Lucassen, F., Harmon, R., Franz, G., Romer, R.L., Becchio, R., Siebel, W., 2002. Lead evolution of the Pre-Mesozoic crust in the Central Andes (18–27°): progressive homogenisation of Pb. Chemical Geology 186, 183–197.

Manhès, G., Minster, J.F., Allègre, C.J., 1978. Comparative uranium–thorium–lead and rubidium–strontium study of the Saint Severin amphoterite: Consequences for early solar system chronology. Earth and Planetary Science Letters 39, 14–24.

Marinovic, N., 1979. Geología de los cuadrángulos Zapaleri y Nevados de Poquis, II Región. Graduate Thesis (unpublished). Universidad de Chile, Santiago. 75 pp.

Miller, C.F., 1985. Are strongly peraluminous magmas derived from pelitic sedimentary sources? Journal of Geology 93, 673–689.

Miller, C.F., Stoddard, E.F., 1981. The role of manganese in the paragenesis of magmatic garnet: an example from the Old Woman Piute Range, California. Journal of Geology 89, 233–246.

Montel, J.M., Vielzeuf, D., 1997. Partial melting of metagreywackes. II. Compositions of minerals and melts. Contributions to Mineralogy and Petrology 128, 176–196.

Morgan VI, G.B., London, D., Luedke, R.G., 1998. Petrochemistry of late-Miocene peraluminous silicic volcanic rocks from the Morococala field, Bolivia. Journal of Petrology 39, 601–632.

Nakamura, N., 1974. Determination of REE, Ba, Fe, Mg, Na and K in carbonaceous and ordinary chondrites. Geochimica et Cosmochimica Acta 38, 757–773.

Nash, W.P., Crecraft, H.R., 1985. Partition coefficients for trace elements in silicic magmas. Geochimica Cosmochimica Acta 49, 2309–2322.

Neiva, A.M.R., Silva, M.M.V.G., Gomes, M.E.P., Campos, T.F.C., 2002. Geochemistry of coexisting biotite and muscovite of portuguese peraluminous granitic differentiation series. Chemie der Erde (Geochemistry) 62, 197–215.

Nekvasil, H., Wen, S., 1994. Solvcalc: an interactive graphics program package for calculating the ternary feldspar solvus and for two-feldspar geothermometry. Computers & Geosciences 20, 1025–1040.

Ort, M., Coira, B., Mazzoni, M., 1996. Generation of a crust–mantle magma mixture: magma sources and contamination at Cerro Panizos, Central Andes. Contributions to Mineralogy and Petrology 123, 308–322.

Patiño Douce, A.E., 1992. Calculated relationships between activity of alumina and phase assemblages of silica-saturated igneous rocks. Petrogenetic implications of magmatic cordierite, garnet and aluminosilicate. Journal of Volcanology and Geothermal Research 52, 43–63.

Patiño Douce, A.E., 1999. What do experiments tell us about the relative contributions of crust and mantle to the origin of granite magmas? In: Castro, A., Fernandez, C., Vigneresse, J.L. (Eds.), Understanding Granites. Integrating New and Classical Techniques: Geological Society of London, Special Publication, 168, pp. 55–75.

Patiño Douce, A.E., Beard, J.S., 1995. Dehydration melting of biotite gneiss and quartz amphibolite from 3 to 15 kbar. Journal of Petrology 36, 707–738.

Patiño Douce, A.E., Harris, N., 1998. Experimental constraints on Himalayan anatexis. Journal of Petrology 39, 689–710.

Patiño Douce, A.E., Johnston, A.D., 1991. Phase equilibria and melt productivity in the pelitic system: implications for the origin of peraluminous granitoids and aluminous granulites. Contributions to Mineralogy and Petrology 107, 202–218.

Pearce, J.A., Norry, M.J., 1979. Petrogenetic implications of Ti, Zr, Y, and Nb variations in volcanic rocks. Contributions to Mineralogy and Petrology 69, 33–47.

Pérez-Soba, C., Villaseca, C., 2010. Petrogenesis of highly fractionated I-type peraluminous granites: La Pedriza pluton (Spanish Central System). Geologica Acta 8, 1–20.

Petrinovic, I.A., Riller, U., Brod, J.A., Alvarado, G., Arnosio, M., 2006. Bimodal volcanism in a tectonic transfer zone: Evidence for tectonically controlled magmatism in the southern Central Andes, NW Argentina. Journal of Volcanology and Geothermal Research 152, 240–252.

Pichavant, M., Valencia Herrera, J., Boulmier, S., Briqueu, L., Joron, J.L., Juteau, M., Maria, L., Michard, A., Sheppard, S.M.F., 1987. The Macusani glasses, SE Peru: evidence of chemical fractionation in peraluminous magmas. Geochemical Society, Special Publication 1, 359–373.

Pichavant, M., Kontak, D.J., Valencia Herrera, J., Clark, A.H., 1988a. The Miocene–Pliocene Macusani volcanics, SE Peru: I. Mineralogy and magmatic evolution of a two-mica aluminosilicate-bearing ignimbrite suite. Contributions to Mineralogy and Petrology 100, 300–324.

Pichavant, M., Kontak, D.J., Briqueu, L., Valencia Herrera, J., Johnston, R.M., 1988b. The Miocene–Pliocene Macusani Volcanics, SE Peru: II. Geochemistry and origin of a felsic peraluminous magma. Contributions to Mineralogy and Petrology 100, 325–338.

Pigage, L.C., Greenwood, H.J., 1982. Internally consistent estimates of pressure and temperature: the staurolite problem. American Journal of Science 282, 943–969.

Pouchou, J.L., Pichoir, F., 1985. "PAP" (B(U)) correction procedure for improved microanalysis. In: Armstrong, J.T. (Ed.), Microbeam Analysis. San Francisco Press, San Francisco, CA, pp. 104–106.

Putirka, K.D., 2005. Igneous thermometers and barometers based on plagioclase and liquid equilibria: tests of some existing models and new calibrations. American Mineralogist 90, 336–346.

Richard, P., Shimizu, N., Allègre, C.J., 1976. $^{143}Nd/^{146}Nd$, a natural tracer: an application to oceanic basalts. Earth and Planettary Science Letters 31, 269–278.

Richardson, S.W., Gilbert, M.C., Bell, P.M., 1969. Experimental determination of kyanite–andalusite and andalusite–sillimanite equilibria: the aluminium silicate triple point. American Journal of Science 267, 259–272.

Rickwood, P.C., 1968. On recasting analyses of garnet into end-member molecules. Contributions to Mineralogy and Petrology 18, 175–198.

Rollinson, H.R., 1993. Using Geochemical Data: Evaluation, Presentation, Interpretation. Longman Scientific & Technical Editions, Singapore. (352 pp.).

Salisbury, M.J., Jicha, B.R., deSilva, S.L., Singer, B.S., Jiménez, N.C., Ort, M.H., 2011. $^{40}Ar/^{39}Ar$ chronostratigraphy of Altiplano–Puna volcanic complex ignimbrites reveals the development of a major magmatic province. Geological Society of America Bulletin 123, 821–840.

Sandeman, H.A., Clark, A.H., 2003. Glass-rich, cordierite–biotite rhyodacite, Valle Ninahuisa, Puno, southeastern Peru: petrological evidence for hybridization of "Lachlan S-type" and potassic mafic magmas. Journal of Petrology 44, 355–385.

Sandeman, H.A., Clark, A.H., 2004. Commingling and mixing of S-type peraluminous, ultrapotassic and basaltic magmas in the Cayconi volcanic field, Cordillera de Carabaya, SE Peru. Lithos 73, 186–213.

Scaillet, B., Holtz, F., Pichavant, M., 1998. Phase equilibrium constraints on the viscosity of silicic magmas 1. Volcanic–plutonic comparison. Journal of Geophysical Research 103, 27257–27266.

Schilling, F.R., Trumbull, R.B., Brasse, H., Haberland, C., Asch, G., Bruhn, D., Haak, V., Giese, P., Mai, K., Munoz, M., Ramelow, J., Rietbrock, A., Ricaldi, E., Vietor, T., 2006. Partial melting in the Central Andean Crust, a review of geophysical, petrophysical, and petrologic evidence. In: Oncken, O., et al. (Ed.), The Andes — Active Subduction Orogeny. : Frontiers in Earth Science Series. Springer-Verlag, Berlin, Heidelberg, New York, pp. 460–474.

Schmitt, A.K., de Silva, S.L., Trumbull, R.B., Emmermann, R., 2001. Magma evolution in the Purico ignimbrite complex, northern Chile: evidence for zoning of a dacitic magma by injection of rhyolitic melts following mafic recharge. Contributions to Mineralogy and Petrology 140, 680–700.

Schneider, A., 1987. Eruptive processes, mineralization and isotopic evolution of the Los Frailes, Kari Kari Region, Bolivia. Revista Geológica de Chile 30, 27–33.

Sola, A., Becchio, R., 2011. Migmatite leucosomes as magma analogues for leucogranites and trondhjemites of the Famatinian belt: a case study from Sierra de Molinos, Salta, NW Argentina. Actas XVIII Congreso Geologico Argentino, Neuquén (CD ROM).

Soler, M.M., 2005. Caldera Vilama (Mioceno Superior): Su estratigrafía, evolución magmática y relación con eventos ignimbríticos tempranos, Puna Argentina–Altiplano Boliviano. Ph.D. Thesis (unpublished). Facultad de Ciencias Naturales, Universidad Nacional de Salta, Argentina. 336 pp.

Stacey, J.S., Kramers, J.D., 1975. Approximation of terrestrial lead isotope evolution by a two-stage model. Earth and Planetary Science Letters 26, 207–221.

Sylvester, P.J., 1998. Post-collisional strongly peraluminous granites. Lithos 45, 29–44.

Tischendorf, G., Gottesmann, B., Förster, H.-J., Trumbull, R.B., 1997. On Li-bearing micas: estimating Li from electron microprobe analysis and an improved diagram for graphical representation. Mineralogical Magazine 61, 809–834.

Vielzeuf, D., Holloway, J.R., 1988. Experimental determination of the fluid-absent melting reactions in the pelitic system (consequences for crustal differentiation). Contributions to Mineralogy and Petrology 98, 257–276.

Vielzeuf, D., Montel, J.M., 1994. Partial melting of metagreywackes. 1. Fluid-absent experiments and phase relationships. Contributions to Mineralogy and Petrology 117, 375–393.

Villaros, A., Stevens, G., Moyen, J.F., Buick, I.S., 2009. The trace element compositions of S-type granites: evidence for disequilibrium melting and accessory phase entrainment in the source. Contributions to Mineralogy and Petrology 158, 543–561.

Villaseca, C., Barbero, L., 1994. Chemical variability of Al–Ti–Fe–Mg minerals in peraluminous granitoids rocks from central Spain. European Journal of Mineralogy 6, 691–710.

Villaseca, C., Orejana, D., Paterson, B.A., 2007. Zr-LREE rich minerals in residual peraluminous granulites, another factor in the origin of low Zr-LREE granitic melts? Lithos 96, 375–386.

Viramonte, J.G., Omarini, R.H., Araña Saavedra, V., Aparicio, A., García Cacho, L., Parica, P., 1984. Edad, génesis y mecanismos de erupción de las riolitas granatíferas de San Antonio de los Cobres, Provincia de Salta. 9° Congreso Geológico Argentino, Actas, 3, pp. 216–233 (Bariloche).

Viramonte, J.M., Viramonte, J.G., Becchio, R., Pimentel, M., Arnosio, M., 2007. Ramadas volcanic centre (NW-Argentina): linking between the Miocene volcanism and the lower Paleozoic basement. 20th Colloquium on Latin American Earth Sciences (LAK). Abstracts, pp. 62–63 (Kiel, Germany).

Watson, E.B., Harrison, T.M., 1983. Zircon saturation revisited: temperature and compositional effects in a variety of crustal magma types. Earth and Planetary Science Letters 64, 295–304.

Wilcox, D., Dove, B., Mc David, D., Greer, D., 2002. Image Tool for Windows. Version 3.0. The University of Texas Health Science Center, San Antonio, Texas, p. 27.

Wyborn, D., Chappell, B.W., Johnston, R.M., 1981. Three S-type volcanic suites from the Lachlan Fold Belt, Southeast Australia. Journal of Geophysical Research 86, 10335–10348.

Zeng, L., Asimow, P.D., Saleeby, J.B., 2005. Coupling of anatectic reactions and dissolution of accessory phases and the Sr and Nd isotope systematics of anatectic melts from a metasedimentary source. Geochimica et Cosmochimica Acta 69, 3671–3682.